

INFORMATION TO USERS

This manuscript has been reproduced from the microfilm master. UMI films the text directly from the original or copy submitted. Thus, some thesis and dissertation copies are in typewriter face, while others may be from any type of computer printer.

The quality of this reproduction is dependent upon the quality of the copy submitted. Broken or indistinct print, colored or poor quality illustrations and photographs, print bleedthrough, substandard margins, and improper alignment can adversely affect reproduction.

In the unlikely event that the author did not send UMI a complete manuscript and there are missing pages, these will be noted. Also, if unauthorized copyright material had to be removed, a note will indicate the deletion.

Oversize materials (e.g., maps, drawings, charts) are reproduced by sectioning the original, beginning at the upper left-hand corner and continuing from left to right in equal sections with small overlaps.

ProQuest Information and Learning
300 North Zeeb Road, Ann Arbor, MI 48106-1346 USA
800-521-0600

UMI[®]

**STATIC AND DYNAMIC STRAIN AGING OF 304
STAINLESS STEEL AT HIGH TEMPERATURES**

By

David Lobo

A Thesis Submitted to the Faculty of Graduate Studies and
Research in Partial Fulfillment of the Requirements for the
Degree of Master of Engineering

Department of Mining and Metallurgical Engineering
McGill University
Montreal, Canada

©David Lobo
November 2000



**National Library
of Canada**

**Acquisitions and
Bibliographic Services**

**395 Wellington Street
Ottawa ON K1A 0N4
Canada**

**Bibliothèque nationale
du Canada**

**Acquisitions et
services bibliographiques**

**395, rue Wellington
Ottawa ON K1A 0N4
Canada**

Your file Votre référence

Our file Notre référence

The author has granted a non-exclusive licence allowing the National Library of Canada to reproduce, loan, distribute or sell copies of this thesis in microform, paper or electronic formats.

The author retains ownership of the copyright in this thesis. Neither the thesis nor substantial extracts from it may be printed or otherwise reproduced without the author's permission.

L'auteur a accordé une licence non exclusive permettant à la Bibliothèque nationale du Canada de reproduire, prêter, distribuer ou vendre des copies de cette thèse sous la forme de microfiche/film, de reproduction sur papier ou sur format électronique.

L'auteur conserve la propriété du droit d'auteur qui protège cette thèse. Ni la thèse ni des extraits substantiels de celle-ci ne doivent être imprimés ou autrement reproduits sans son autorisation.

0-612-70241-3

Canada

ABSTRACT

Distinct yield drops and serrations were observed on the stress-strain curves of a 304 type stainless steel when tested at high temperatures (850-1200°C). A proposed explanation for this behavior is static strain aging (SSA) and dynamic strain aging (DSA), respectively, caused by the presence of substitutional elements.

Much of the previous work on this topic has been focused on the effects of interstitials, namely carbon and nitrogen, at lower temperatures (100-300 °C, depending on the strain rate). However, for substitutional elements to have the same effect, the temperature range must be significantly higher. To further investigate the likelihood that SSA and DSA are caused by substitutional elements, the domain (i.e. temperature and strain rate range) within which yield drops and serrated yielding are observed was studied.

The results of this investigation showed that the appearance of SSA is dependent upon the pass strain, interpass time and strain rate, whereas the presence of DSA serrations was strongly dependent upon strain rate. The disappearance of yield drops involves interpass times in excess of one second. This is hypothesized to result from the disappearance of the deformation vacancies and of the associated non-equilibrium segregation. The impurity element phosphorus was isolated as the most probable cause of the observed phenomenon. This is a result of its high diffusivity, combined with its high binding energy.

RÉSUMÉ

Lors de la déformation à chaud d'échantillons en acier inoxydable, on observe des oscillations en dents de scie sur les courbes contraintes-déformation. Ces oscillations de la contrainte d'écoulement sont expliquées par les effets du vieillissement statique et dynamique des aciers.

La plupart des travaux sur ce sujet se sont intéressés aux basses températures (100-300°C, suivant la vitesse de déformation) et à l'effet des éléments interstitiels tel le carbone et l'azote. Cependant, pour que les éléments de substitution aient le même effet, des températures plus élevées sont nécessaires. Ainsi, pour étudier l'éventuelle relation entre ces éléments et les phénomènes de vieillissement, le domaine de température et de vitesse de déformation pour lesquels les oscillations sont présentes a été étudié.

Les résultats montrent que le vieillissement statique est fonction du montant de déformation, du temps entre les incréments de déformation, et de la vitesse de déformation. La disparition des oscillations, pour des temps d'arrêts excédant une seconde, coïncide avec la disparition des lacunes induites par la déformation et la ségrégation hors d'équilibre. Le phosphore est probablement l'agent responsable de ce phénomène, due à sa grande diffusivité et sa forte énergie de liaison.

ACKNOWLEDGEMENTS

I would like to thank my supervisor, Professor John J. Jonas, for giving me the opportunity to work with him. His collaboration and interest throughout the course of this study were very helpful. I would also like to thank Professor René Le Gall for his innovative ideas and suggestions. Their help was greatly appreciated.

I would also like to thank Laurent Gavard and Mr. Daniel Bélanger of Atlas Stainless Steel in Tracy, Quebec for providing the material necessary to conduct these experiments. I would also like to recognize Edwin Fernandez, for all his help in the laboratory, and Abdelbaset Elwazri for his extensive knowledge and aid in operating the laboratory equipment. I cannot forget Lorraine Mello for all her administrative help throughout the years.

I am also grateful to all the friends that I have made. This includes my office mates, both past and present, as well as all the friends that I have made within and outside the department. They have been very helpful and have made my years at McGill thoroughly enjoyable. Last, and not least, I would like to express my heartfelt gratitude to my family: Mom, Dad, Belinda and Cassandra. Their love and guidance have made everything that I have accomplished possible.

TABLE OF CONTENTS

ABSTRACT	i
RÉSUMÉ	ii
ACKNOWLEDGEMENTS	iii
TABLE OF CONTENTS	iv
LIST OF FIGURES	vi
LIST OF TABLES	ix
CHAPTER 1 INTRODUCTION	1
CHAPTER 2 LITERATURE REVIEW	4
2.1 STATIC STRAIN AGING	4
2.2 DYNAMIC STRAIN AGING	7
2.2.1 APPEARANCE AND DISAPPEARANCE OF DYNAMIC STRAIN AGING SERRATIONS	10
2.2.2 TYPES OF DYNAMIC STRAIN AGING SERRATIONS	12
2.2.3 CRITICAL STRAIN	13
2.2.4 OTHER MANIFESTATIONS OF DYNAMIC STRAIN AGING	16
2.3 THE EFFECT OF CHEMICAL COMPOSITION ON STRAIN AGING	19
2.4 PRACTICAL IMPLICATIONS OF STRAIN AGING	20
2.5 CONTROLLING STRAIN AGING	21
2.6 STRAIN AGING CAUSED BY SUBSTITUTIONAL ELEMENTS IN STEEL	22
2.7 SUMMARY	25
CHAPTER 3 EXPERIMENTAL DETAILS	26
3.1 MATERIALS	26
3.2 UNIAXIAL COMPRESSION TESTING	27
3.2.1 SPECIMEN PREPARATION	27
3.2.2 COMPRESSION TESTING SYSTEM	28
3.2.3 COMPRESSION TOOLS	28

Table of Contents

3.2.4	FURNACE AND TEMPERATURE CONTROL	28
3.3	DATA ACQUISITION AND PROCESSING	30
3.4	THERMOMECHANICAL PROCESSING (TMP) SCHEDULE	31
3.5	TYPES OF TESTS	32
3.5.1	SIMPLE COMPRESSION TESTS	32
3.5.2	STRAIN RATE CHANGE TESTS	33
CHAPTER 4	RESULTS AND DISCUSSION	34
4.1	SIMPLE COMPRESSION RESULTS FOR STEEL A	34
4.1.1	THE EFFECT OF PASS STRAIN	40
4.1.2	THE EFFECT OF INTERPASS TIME	45
4.1.3	THE EFFECT OF STRAIN RATE	50
4.2	ELEMENTS RESPONSIBLE FOR THE STATIC AND DYNAMIC STRAIN AGING	53
4.2.1	DIFFUSION CALCULATIONS	56
4.3	SIMPLE COMPRESSION RESULTS FOR STEEL B	59
4.4	ENHANCED DIFFUSION	63
4.5	COMPLEX FORMATION AND NON-EQUILIBRIUM SEGREGATION	64
4.6	STRAIN RATE CHANGE RESULTS	65
CHAPTER 5	CONCLUSIONS	69
	REFERENCES	73

LIST OF FIGURES

CHAPTER 2 LITERATURE REVIEW

- Figure 2.1 Stress-strain curve for low carbon steel showing strain aging⁷. 5
- Figure 2.2 Schematic representation of the appearance and disappearance of serrations¹⁵. 7
- Figure 2.3 Stress-velocity diagram for a mobile dislocation in the presence of impurities¹⁶. 9
- Figure 2.4 Temperature and strain rate range over which serrations are observed²². 11
- Figure 2.5 Types of serrations commonly observed in deformation of substitutional solid solution alloys². 13
- Figure 2.6 Variation of critical strain with strain rate and temperature². 14
- Figure 2.7 Schematic diagram of the various manifestations of DSA². 16
- Figure 2.8 Stress versus temperature curves showing a comparison of materials that do and do not exhibit DSA³⁵. 18
- Figure 2.9 Stretcher strains on a steel sheet stretched past the yield point³⁹. 21
- Figure 2.10 Diffusion coefficients of the interstitial and substitutional elements in iron⁴⁰. 24

CHAPTER 3 EXPERIMENTAL DETAILS

- Figure 3.1 Schematic diagram of the compression testing machine⁴². 29
- Figure 3.2 Schematic diagram of the TMP schedule employed. 31
- Figure 3.3 Schematic diagram of the deformation cycle employed during the strain rate change tests. 33

CHAPTER 4 RESULTS AND DISCUSSION

- Figure 4.1 (a) Stress-strain curve at 800°C, for a pass strain of 0.2, an

List of Figures

	interpass time of 0.01 s and a strain rate of 0.5 s^{-1} ; (b) magnification of the circled region.	35
Figure 4.2	(a) Stress-strain curve at 1000°C , for a pass strain of 0.2, an interpass time of 0.01 s and a strain rate of 0.5 s^{-1} ; (b) magnification of the circled region.	36
Figure 4.3	(a) Stress-strain curve at 1200°C , for a pass strain of 0.2, an interpass time of 0.01 s and a strain rate of 0.5 s^{-1} ; (b) magnification of the circled region.	37
Figure 4.4	Stress-strain curves at 850, 900 and 950°C showing the appearance of serrations.	38
Figure 4.5	Stress-strain curves obtained using a pass strain of 0.1; strain rate = 0.5 s^{-1} ; interpass time = 0.01 s.	41
Figure 4.6	Stress-strain curves obtained using a pass strain of 0.4; strain rate = 0.5 s^{-1} ; interpass time = 0.01 s.	41
Figure 4.7	Magnified stress-strain curve determined at 1000°C using pass strains of 0.1 showing the presence of DSA serrations.	44
Figure 4.8	Magnified stress-strain curve determined at 1000°C using pass strains of 0.4 showing the presence of DSA serrations.	45
Figure 4.9	Stress-strain curves determined at 900°C and 0.5 s^{-1} using a pass strain of 0.2. Interpass times ranging from 0.01 to 10 s were employed.	46
Figure 4.10	Stress-strain curves determined at 1000°C and 0.5 s^{-1} using a pass strain of 0.2. Interpass times ranging from 0.01 to 20 s were employed.	46
Figure 4.11	Stress-strain curves determined at 1100°C and 0.5 s^{-1} using a pass strain of 0.2. Interpass times ranging from 0.01 to 10 s were employed.	47
Figure 4.12	Stress-strain curve determined using a strain rate of 0.01 s^{-1} with a pass strain of 0.2 and a 0.01 s interpass time.	50
Figure 4.13	Stress-strain curve determined using a strain rate of 1 s^{-1} with a pass strain of 0.2 and a 0.01 s interpass time.	51
Figure 4.14	Stress-strain curve determined using a strain rate of 5 s^{-1} with a pass strain of 0.2 and a 0.01 s interpass time.	51

List of Figures

Figure 4.15	Mean distances travelled by Cr and Ni atoms during the experimental interpass times.	58
Figure 4.16	Mean distances travelled by P atoms during the experimental interpass times.	58
Figure 4.17	Stress-strain curve of steel B determined at 900°C; strain rate = 0.5 s ⁻¹ ; pass strain = 0.2; interpass time = 0.01s.	60
Figure 4.18	Stress-strain curve of steel B determined at 1000°C; strain rate = 0.5 s ⁻¹ ; pass strain = 0.2; interpass times = 0.01 and 1 s.	60
Figure 4.19	Stress-strain curve of steel B determined at 1100°C; strain rate = 0.5 s ⁻¹ ; pass strain = 0.2; interpass times = 0.01 and 1 s.	61
Figure 4.20	Stress-strain curve of steel B determined at 1200°C; strain rate = 0.5 s ⁻¹ ; pass strain = 0.2; interpass time = 0.01s.	61
Figure 4.21	Time dependence of the excess vacancy concentration ⁴⁸ .	64
Figure 4.22	Stress-strain curves determined in the strain rate change tests: 0.5 to 1 and then back to 0.5 s ⁻¹ .	66
Figure 4.23	Stress-strain curves determined in the strain rate change tests at 1000°C: 0.5 to 5 and then back to 0.5 s ⁻¹ .	66
Figure 4.24	Stress-strain curves determined in the strain rate change tests at 1000°C: 0.5 to 0.05 and then back to 0.5 s ⁻¹ .	67

LIST OF TABLES

CHAPTER 3 EXPERIMENTAL DETAILS

Table 3.1 Chemical compositions of the experimental steels in wt%. 26

CHAPTER 4 RESULTS AND DISCUSSION

Table 4.1 Amounts of softening (%) taking place during the interpass times. 48

Table 4.2 Binding energies between solute atoms and grain boundaries in $\gamma\text{-Fe}^{47}$. 55

CHAPTER 1

INTRODUCTION

There are two types of strain aging that can be characterized. Aging that takes place after straining is termed “static strain aging (SSA)” while the term “dynamic strain aging (DSA)” is used to describe the process by which aging and straining occur simultaneously. In both these processes, the changes in mechanical properties are similar in nature in any given system¹⁻³. Typical changes include an increase in the flow stress and work hardening rate accompanied by a decrease in the material’s ductility. In both cases, the strengthening effects are a result of the interaction between solute atoms and dislocations.

In the case of static strain aging, the material has been plastically deformed and is then allowed to age for a certain period of time. During this aging period, the solute atoms are able to diffuse to dislocations and form atmospheres, known as Cottrell atmospheres. These solute atmospheres effectively pin the dislocations, preventing them from continuing their motion upon further loading. Consequently, a higher stress is required to liberate these locked dislocations from their solute atmospheres. The result is an increase in the yield strength of the aged material. In the case of steel, the aging

effects are attributed to the interstitial elements carbon and nitrogen. This is due to the fact that interstitial elements possess a significantly higher diffusivity than do substitutional elements. Since solute atoms must diffuse through the lattice to accumulate around dislocations, strain aging becomes a time dependent phenomenon. It is also temperature dependent due to the fact that the diffusivity is strongly dependent on temperature.

In the case of dynamic strain aging, the solute atoms must possess enough mobility to interact with moving dislocations. During deformation, dislocation motion becomes temporarily arrested at local obstacles, at which time solute atoms are able to diffuse to the dislocations and pin them². During continued deformation, the dislocations break free of the solute atoms and the process is repeated. The continuous pinning and unpinning of dislocations creates “jerky flow” on a stress-strain curve. This is also known as “serrated yielding” or the “Portevin-Le Chatelier Effect”⁴. Since the occurrence of DSA develops as the diffusivities of solute atoms approach the dislocation velocity, the effects are dependent upon temperature and strain rate. This is because the diffusivities of solute atoms are a strong function of temperature while the dislocation velocity is governed by the imposed strain rate.

While serrated yielding remains the most visible evidence of DSA, other effects are attributable to the presence of DSA as well. Additional manifestations of DSA are a peak in the flow stress and work hardening rate as well as a negative strain rate sensitivity dependence of the flow stress. These effects have been reported to occur over a wider range of temperature and strain rate than does serrated yielding^{2,3}.

Much of the previous work on SSA and DSA has focused on the effects of interstitial elements in steels. These effects are known to take place at low temperatures, within the blue brittle region (i.e. at temperatures ranging between 100 and 300°C). The effect of substitutional elements has been studied in the case of aluminum and zinc alloys. However, the effect of the substitutional elements contained in steel on the presence of SSA and DSA has yet to be fully explored. In certain cases, researchers have reported

evidence of DSA as a result of substitutional atoms^{5,6}. In these experiments, serrated yielding was found to occur over the temperature range 900-1200°C at various strain rates. Due to the high temperatures involved in these experiments, it was readily apparent that the diffusion rates of the interstitial elements would be too high to contribute to any DSA effects. Therefore, it was proposed that substitutional elements could be responsible for the DSA effects⁵. In one case reported by Bai *et al.*, the substitutional element Nb was believed to be responsible for the DSA effects observed⁶.

In what follows, **Chapter 2** presents a literature review describing the basic theories behind the processes of static strain aging and dynamic strain aging as they pertain to steel. In addition, the pertinent work of various researchers over the last forty years will be presented in order to give the reader a better understanding of the topic.

The objectives, experimental procedures and materials used are outlined in **Chapter 3**. This chapter also provides a brief discussion of the testing methods employed during the study. The experimental results are presented in **Chapter 4** and the results are then discussed, providing an explanation for the effects observed. Finally, the conclusions drawn from this study are outlined in **Chapter 5**.

CHAPTER 2

LITERATURE REVIEW

2.1 STATIC STRAIN AGING

Aging that takes place after straining is referred to as static strain aging (SSA). The behavior is illustrated in **Figure 2.1**, which schematically describes the effects of strain aging on the tensile stress-strain curve of low carbon steel. Region A depicts the stress-strain curve for a typical low carbon steel exhibiting an upper and lower yield point. As proposed by Cottrell, the yield point phenomenon is the result of interactions between dislocations and solute atoms⁸. Solute atoms form atmospheres around dislocations, thereby pinning or anchoring them. Additional stress is then required to free these dislocations for movement, thus the presence of the higher stress “upper yield point”. The “lower yield point” then represents the stress required for continued dislocation motion; the latter results in what is also known as the Lüders strain. As previously stated, the main elements responsible for aging effects in steel are carbon and

nitrogen. This is a result of the much higher diffusivities of interstitial elements as compared to substitutional elements.

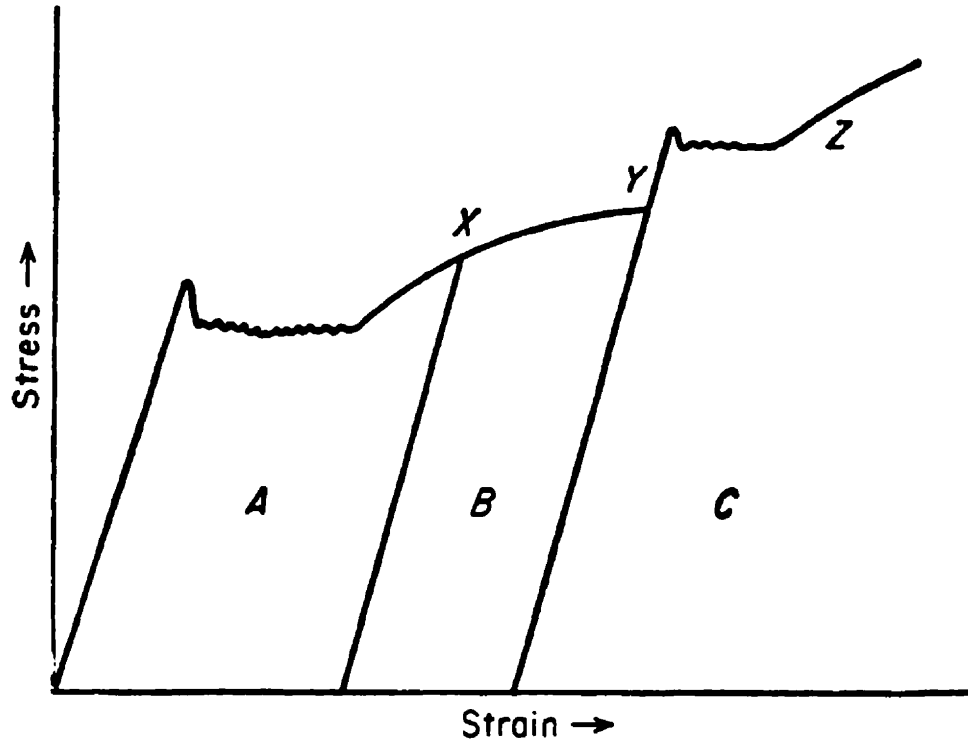


Figure 2.1: Stress-strain curves for low carbon steel showing strain aging⁷.

If the specimen is strained through region A up to a point X, unloaded and then immediately retested, a stress-strain curve such as that shown in region B is obtained. It is important to note that the yield point is no longer visible. This can be explained by the fact that the dislocations are no longer locked in place by the solute atmospheres. However, the yield strength has increased. Now consider the case where the specimen is strained to point Y and then unloaded. If the specimen is allowed to age at room temperature or above for a certain period of time and then reloaded, the result is the stress-strain curve in region C. The yield point reappears at a higher stress as a consequence of the aging effects. The reappearance of the yield point is caused by the

diffusion of the carbon and nitrogen atoms to the dislocations. This, in turn, leads to the formation of new solute atmospheres that once again pin the dislocations and restrict further motion.

Proof of the contribution of carbon and nitrogen to strain aging effects has been previously presented by various investigators⁹⁻¹¹. It was shown that the activation energy corresponding to the return of the yield drop after aging is approximately equal to the activation energy required for the diffusion of carbon and nitrogen in steel; this will be discussed in a subsequent section. It is also important to note that nitrogen will contribute more towards strain aging in steel than will carbon. This is a result of its higher solubility and diffusion coefficient in steel. Nitrogen also possesses a high binding energy to dislocations, meaning that dislocations will have greater difficulty in escaping from an atmosphere composed of nitrogen atoms.

Although the most noticeable effect of static strain aging is the increase in yield stress after aging, other properties are also affected. This includes the ultimate tensile strength, the ductile-to-brittle transition temperature, high temperature strength, fatigue strength and the electrical and magnetic properties of steel⁹. An explanation for the change in mechanical properties was proposed by Hundy and by Wilson and Russell^{9,12-14}. They proposed that the aging process took place in two stages. In the first stage, it is believed that the solute atoms diffuse to dislocations, forming atmospheres, thereby locking the dislocations in place. This stage results in an increase in the yield stress and Lüders strain and a subsequent decrease in the ductile-to-brittle transition temperature. The second stage of the aging process involves the formation of precipitates along the dislocations. This is because dislocations are known to be very effective nucleation sites, so solute atoms are able to precipitate in the presence of dislocations but not in their absence. During stage two, the yield stress continues to rise and the transition temperature continues to fall. However, the Lüders strain remains relatively constant. Also, the precipitates contribute to the overall strength of the steel and therefore an increase in the ultimate tensile strength and work hardening rate are also seen, accompanied by a decrease in the elongation to fracture and reduction in area. If the

concentration of the solute atoms is too low to allow for precipitation effects, only stage one is observed.

2.2 DYNAMIC STRAIN AGING

The process whereby aging takes place as a material is being strained is known as dynamic strain aging (DSA). As is the case for SSA, DSA also involves interactions between solute atoms and dislocations. DSA occurs when solute atoms gain enough mobility to interact with moving dislocations. Once the solute atoms reach the dislocations, they begin to form solute atmospheres (as was the case for SSA) and thereby restrict dislocation motion. Since the material is flowing continuously, the dislocations eventually obtain enough energy to break free of their solute atmospheres and the process is repeated. This continuous pinning and unpinning of dislocations results in "jerky flow" on a stress-strain curve, as seen in **Figure 2.2**, commonly referred to as serrated yielding. Serrated yielding is the most commonly observed macroscopic manifestation of DSA. This phenomenon is also referred to as the Portevin-LeChatelier or PLC effect after the original investigators of this phenomenon in aluminum alloys^{2,3,10}.

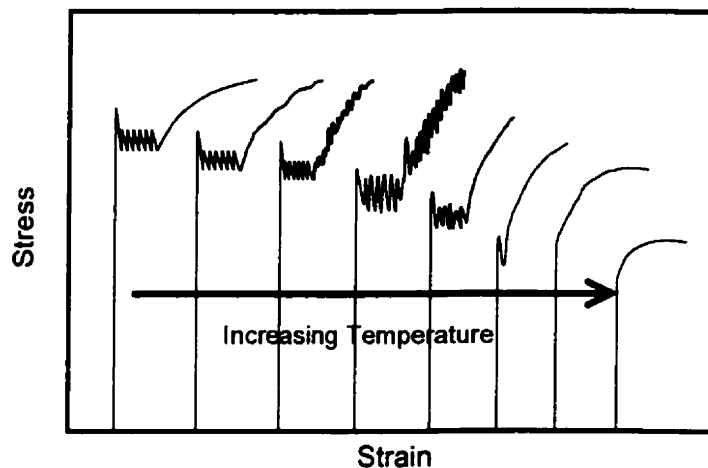


Figure 2.2: Schematic representation of the appearance and disappearance of serrations¹⁵.

Several theories have been devised in order to explain DSA. As previously stated, DSA refers to the interaction of a diffusing solute species and mobile dislocations.

Originally, most theories assumed that this interaction occurred during the free flight motion of dislocations. More recent theories have proposed that aging during deformation occurs, not during the uninhibited motion of dislocations, but during arrest periods, where motion is temporarily halted^{1,2}. At this time, solute atoms are able to segregate to the dislocations and form solute atmospheres, once again known as Cottrell atmospheres. These atmospheres induce a drag force on the dislocations, slowing them even further. Therefore, a higher stress is required to produce dislocation motion. Once this occurs, dislocations speed up and escape the solute atmospheres and once again they proceed without inhibition until another obstacle is reached.

The mechanisms of solute drag and solid solution hardening can be described by use of the catastrophe theory¹⁶, as depicted schematically in **Figure 2.3**. The presence of impurity atoms greatly increases lattice friction and the force exerted on the dislocations as a result of the increased lattice friction increases with increasing dislocation velocity; this is indicated by *curve (1)*. The drag force experienced by dislocations moving with solute atmospheres in tow increases rapidly with increasing velocity, *curve (2)*. *Curve (3)* indicates the concentration of diffusing solute atoms; this can be seen to decrease rapidly with increasing dislocation velocity. *Curve (4)* illustrates the behavior of dislocations as a result of DSA. At low speeds, $V < V_M$, and the dislocations are said to be within the drag regime. In this regime, the solute atoms/atmospheres surrounding the dislocations are able to move along with them. The velocity continues to increase until it exceeds V_M , at which point the dislocations begin to break free from their surrounding atmospheres. The solute drag force decreases until it reaches a stabilizing velocity, V_3 , governed by the applied stress, F_M . The dislocations are then completely free from their solute atmospheres. The free moving dislocations travel through the lattice and eventually encounter obstacles, which begin to slow them down. Such obstacles include dislocation substructures, precipitates and grain boundaries. Eventually, the velocity returns to V_M and the dislocations re-enter the instability regime. Solute atoms are, once again, able to segregate to these dislocations and form new solute atmospheres. This will further increase the drag force and the velocity will return to its starting point V_1 , at which point the process is repeated.

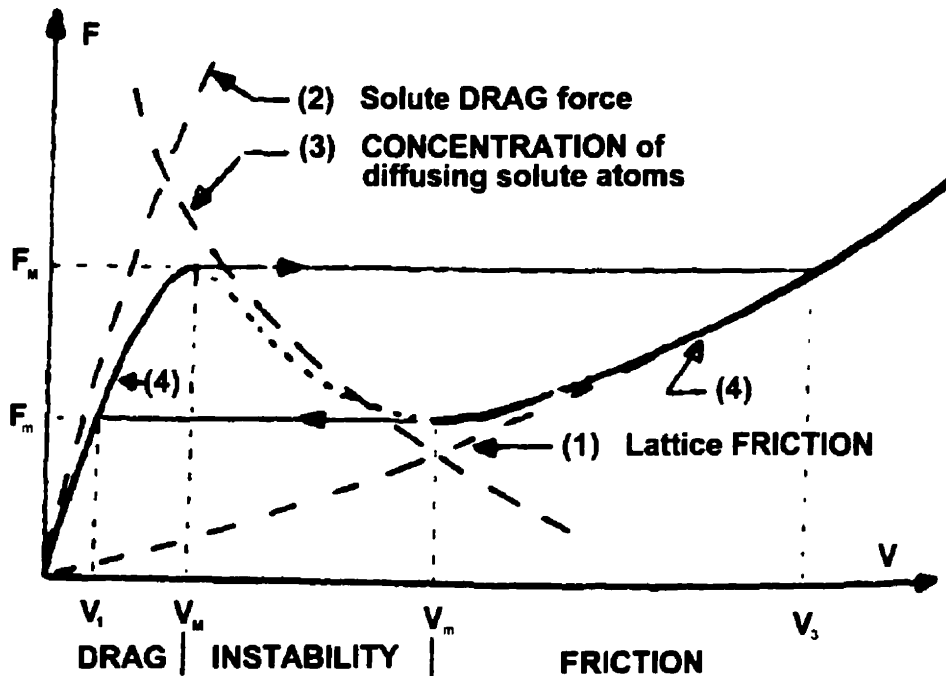


Figure 2.3: Stress-velocity diagram for a mobile dislocation in the presence of impurities¹⁶.

The idea that pinning occurs when dislocations are arrested was further examined by Rubiolo and Bozzano as well as by various other authors¹⁷⁻¹⁹. In fact, their theory better serves to explain the presence of "jerky flow" on a stress-strain curve since it recognizes the fact that dislocation motion is jerky (discontinuous glide) and not continuous (viscous glide). As dislocations glide throughout the lattice, they will encounter obstacles that temporarily disrupt their motion. For such a process, the average dislocation velocity can be expressed in terms of an arrest or waiting time, t_w , and a time of movement through the lattice to reach the next obstacle, t_f :

$$\bar{v} = \frac{\lambda_a}{t_w + t_f} \quad (1)$$

where λ_a is the average distance between obstacles. If the arrest time is sufficiently long, dislocations may be pinned or locked by nearby solute atoms. A higher stress is then required to liberate these dislocations. This results in the discontinuous, jerky flow or serrated yielding present on the stress-strain curve.

Still another theory explains the effects of DSA through dislocation generation^{20,21}. As is widely believed, as dislocations travel through the lattice, solute atoms with sufficient mobility are able to keep up with them and consequently pin or lock them. In this case, the pinned dislocations are restricted from further movement. In order to maintain the imposed strain rate, it becomes easier to activate fresh dislocations rather than unpin locked dislocations. This theory is now generally accepted as an explanation of the increased work hardening rate in the case of interstitial alloys²¹.

2.2.1 APPEARANCE AND DISAPPEARANCE OF DYNAMIC STRAIN AGING SERRATIONS

Temperature and strain rate play an important role in the presence of DSA. The diffusion coefficient varies exponentially with temperature, as seen in the following equation:

$$D = D_0 \exp\left(-\frac{Q_d}{RT}\right) \quad (2)$$

where D_0 is a temperature-independent pre-exponential, Q_d is the activation energy for diffusion, R is the gas constant and T is the absolute temperature. Therefore, increasing the temperature will increase the diffusivity of the solute atoms. Strain rate governs the dislocation velocity. Increasing the strain rate increases the dislocation velocity and shortens the arrest period at obstacles. The dependence of the appearance and disappearance of serrations on temperature and strain rate can be expressed by means of an Arrhenius type equation²²:

$$\dot{\epsilon} = A \exp\left(\frac{-Q}{RT}\right) \quad (3)$$

where $\dot{\epsilon}$ is the strain rate, A is a frequency factor, Q is the activation energy, R is the gas constant and T the absolute temperature^{4,23}. By plotting the strain rate versus the inverse absolute temperature, one can determine the strain rate and temperature range within which serrations appear (**Figure 2.4**). The completely filled squares represent fully serrated stress-strain curves, the open squares indicate perfectly smooth curves while the partially filled squares are associated with curves displaying an intermediate degree of serrations.

In **Figure 2.4**, three distinct regions can be observed relating to the presence or absence of serrations. In the first region, A, at low temperatures, solute atoms do not have enough mobility to keep up with dislocations and so, dislocations move unhindered through the lattice. Solute atoms in the second region, B, at very high temperatures, move rapidly and are able to travel in phase²⁴ with the dislocations, not hindering movement. At intermediate temperatures, the middle region (C), mobile solute atoms interact with moving dislocations as previously discussed. This region is known as the DSA or PLC region. As the strain rate is increased, the DSA region can be seen to shift to higher temperatures. This was also clearly observed in the work of Karimi Taheri *et al.*²², where the temperature range was seen to increase when the strain rate was increased from 10^{-4} to 10^{-1} s^{-1} .

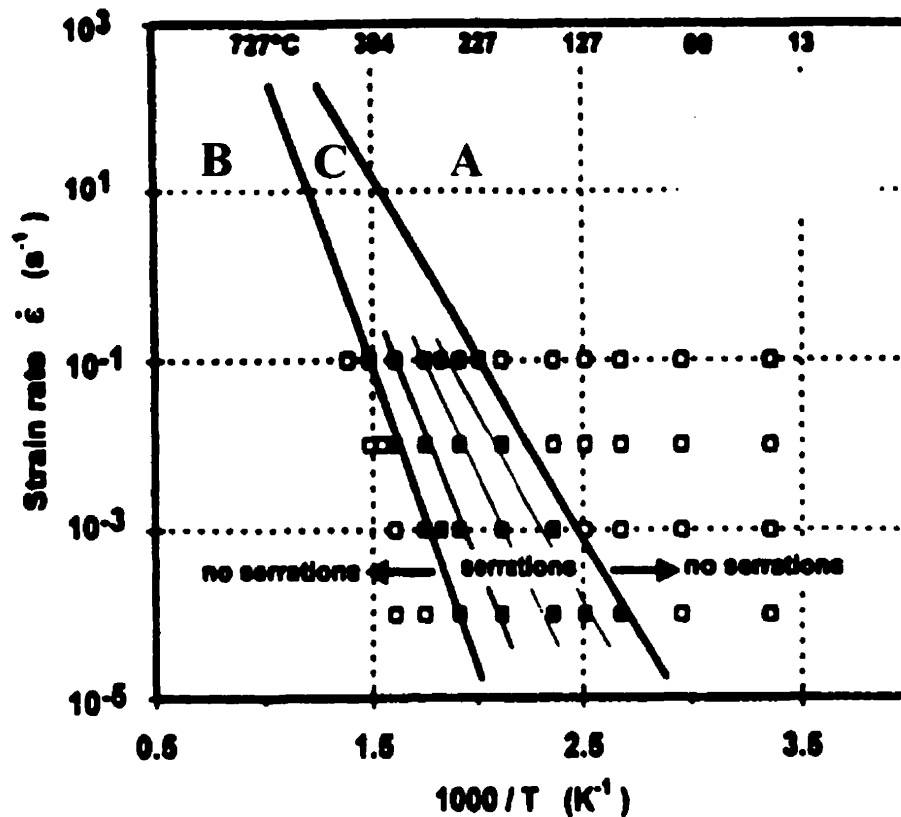


Figure 2.4: Temperature and strain rate range over which serrations are observed²².

There are two heavy lines that bound the DSA region. The slopes of these lines are associated with the mechanisms responsible for the appearance and disappearance of the serrations. The line on the right denotes the appearance of the serrations as the temperature is increased. The activation energy for the appearance of serrations is approximately equal to 84 kJ/mole¹. It has been reported that the activation energy associated with the appearance of serrations, Q_D , is related to the activation energy of the diffusing species, i.e., it is similar to that for the diffusion of carbon and nitrogen ($Q_D = 75\text{-}85$ kJ/mole)^{1,9,10,22,25}. The line on the left represents the disappearance of the serrations as the temperature is increased and the slope of the line can be seen to be higher than the slope of the line for the appearance of the serrations. It has been proposed by Keh *et al.*¹⁰ that the higher activation energy for the disappearance of serrations is associated with the binding energy of the interstitial atoms to the dislocation core (~ 50 kJ/mole). Therefore, the activation energy for the disappearance of serrations is a combination of two energies:

$$Q_f = Q_D + U_C \quad (4)$$

where Q_D is the activation energy for the diffusing solute species and U_C is the binding energy. Various methods of calculating the activation energy for the appearance and disappearance of serrations are outlined in a paper by de Almeida and Emygdio²⁶.

2.2.2 TYPES OF DYNAMIC STRAIN AGING SERRATIONS

The serrations on stress-strain curves attributable to interstitial elements are found to be irregular and not easily analyzed². However, those associated with the interaction of substitutional elements and dislocations can be classified into five categories, depending on their appearance and the experimental conditions that produce them^{2,27}. **Figure 2.5** illustrates the different types of serrations. Type A, B and C serrations are well known and have also been well documented, whereas types D and E have only been more recently observed²⁷.

Type A serrations result from the propagation of shear bands along the gauge length of the specimen. They are known as locking serrations and occur in the low temperature, high strain rate part of the DSA region. Type B serrations are a result of

discontinuous band propagation. They develop from type A serrations with increasing strain or they occur at high temperatures and low strain rates. Type C serrations are considered to be a result of dislocation unlocking. They generally occur at higher temperatures and lower strain rates than the type A and B serrations. Type D serrations are due to band propagation like the type A ones; however, there is less evidence of work hardening. Type E serrations are type A serrations at high strains. They are similar to type A serrations but with little or no work hardening during band propagation. It is important to note that a stress-strain curve is not limited to only one type of serration at a time. As seen in the inset in **Figure 2.5**, type A and B serrations as well as type D and B serrations occur concurrently.

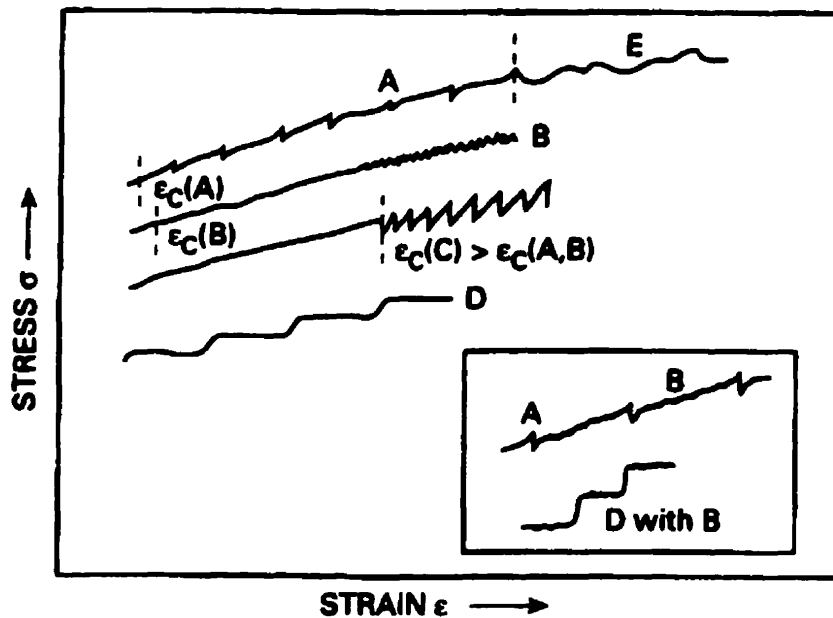


Figure 2.5: Types of serrations commonly observed in deformation of substitutional solid solution alloys².

2.2.3 CRITICAL STRAIN

It is found that a critical strain is required for the onset of serrations in a substitutional alloy^{2,27-29}. This critical strain, ϵ_c , is dependent on both strain rate and temperature, as seen in **Figure 2.6**. At high strain rates and low temperatures, where type

A or B serrations occur, ϵ_c can be seen to increase with increasing strain rate and decreasing temperature. At low strain rates and high temperatures, where type C serrations are observed, ϵ_c increases with decreasing strain rate and increasing temperature. It has also been observed that ϵ_c generally increases with increasing grain size^{2,27,30,31}. This is due to the fact that as a grain increases in size, the number of dislocations decreases. Therefore, more strain must be applied to provide the same number of dislocations as would be present within smaller grains.

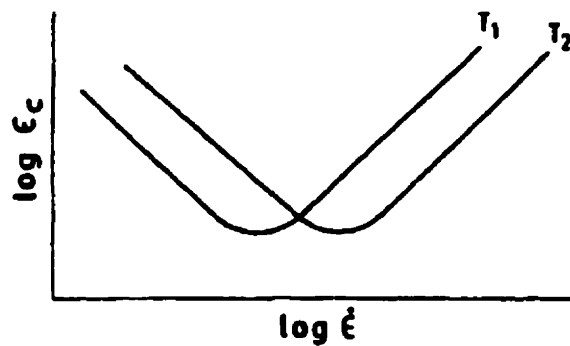


Figure 2.6: Variation of critical strain with strain rate and temperature².

The critical strain serves as an explanation for the discrepancies in the measured diffusion coefficient and that required for the DSA of moving dislocations in substitutional alloys. In essence, DSA was found to occur at lower temperatures than theoretically predicted. The presence of ϵ_c can be related to the requirement that a critical minimum concentration of vacancies be generated during deformation. This concentration of vacancies greatly enhances the diffusion coefficient of the solute species responsible for DSA. An alternative explanation was proposed by Cuddy and Leslie²⁴. They suggested that the DSA observed at lower temperatures was a result of pipe diffusion along dislocations and not vacancy enhanced diffusion. Pipe diffusion raised the diffusivity and allowed for the redistribution of solute atoms at much lower temperatures.

In accordance with the aforementioned theories of the existence of a critical strain, various theoretical models were created based on the interaction of diffusing solute atoms and mobile dislocations²⁷. In all the models, the final result was that, at ϵ_c :

$$\rho_m C_v = K_1 \dot{\epsilon} \exp\left(\frac{E_m}{RT}\right) \quad (5)$$

where C_v is the vacancy concentration, E_m is the vacancy migration energy, T is the absolute temperature and K_1 is a constant. The vacancy concentration varies with strain according to the following equation:

$$C_v = A \epsilon^m \quad (6)$$

where the constant A was found to be 10^{-4} [2]. Similarly, the strain dependence of the mobile dislocation density can be expressed as follows:

$$\rho_m = B \epsilon^\beta \quad (7)$$

where B and β are constants. From equations (5), (6) and (7), the critical strain can be expressed in terms of strain rate and temperature according to the following equation:

$$\epsilon_c^{m-\beta} = K_2 \dot{\epsilon} \exp\left(\frac{E_m}{RT}\right) \quad (8)$$

Experimental results in the low temperature-high strain rate region have yielded reasonable values for m and β . Typical values of $(m+\beta)$ are between 2 and 3 for substitutional alloys and between 0.5 and 1 for interstitial alloys^{26,32}. The aforementioned derivation basically explains that the existence of a critical strain is due to the fact that the bulk diffusion of substitutional solute atoms is enhanced by the creation of vacancies during deformation. Therefore, a material must be initially strained to a such point that the diffusion of solute atoms is sufficiently enhanced by the presence of vacancies to permit DSA to take place.

Another alternate interpretation of ϵ_c is that it is the value at which the strain rate sensitivity (SRS) becomes negative^{2,33}. The possible occurrence of more than one critical strain within a single experiment should also be noted². The recent model of Kubin and Estrin deals with ϵ_c in terms of a strain dependence of both the mobile and forest dislocation densities³⁴.

2.2.4 OTHER MANIFESTATIONS OF DYNAMIC STRAIN AGING

As previously mentioned, serrated yielding is the most commonly observed macroscopic manifestation of DSA. However, there are various other phenomena that indicate the presence of DSA in concurrence with serrated yielding. Other manifestations of DSA have recently been described by Robinson and Shaw and by Rodriguez^{2,27} and can be seen in **Figure 2.7**. The various manifestations of DSA are a peak or plateau in the strength, σ ; a peak in the work hardening rate, θ ; negative strain rate sensitivity, γ ; a peak in the Hall-Petch constant, K_e ; and a ductility minimum within the DSA region. Unlike serrated yielding, these parameters are not visible on the stress-strain curve but are derived from the flow stress at a particular strain. They are dependent upon the interactions between dislocations during deformation².

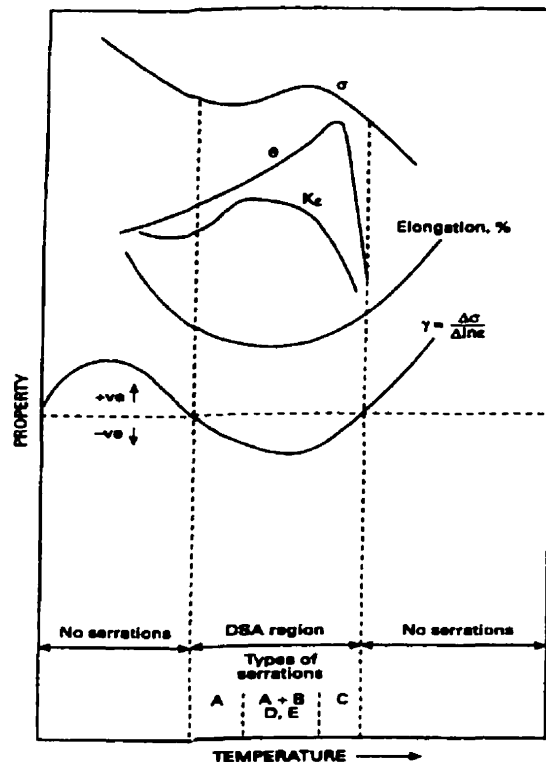


Figure 2.7: Schematic diagram of the various manifestations of DSA².

The yield stress, σ_{ys} , can be considered to be the initial strength of the material prior to any work or strain hardening and the flow stress, σ_e , can be considered to be the

yield stress of the strain hardened material. The strain hardening contribution to the flow stress is then determined as follows:

$$\Delta\sigma = \sigma_{\epsilon} - \sigma_{ys} \quad (9)$$

The strain hardening contribution can be considered to be the sum of various contributions resulting from dislocation interactions. Therefore, the increase in flow stress can be expressed as:

$$\Delta\sigma = \Delta\sigma_{dd} + \Delta\sigma_{dp} + \Delta\sigma_{ds} \quad (10)$$

where $\Delta\sigma_{dd}$ is the stress contribution from dislocation-dislocation interactions, $\Delta\sigma_{dp}$ is the stress contribution from dislocation-precipitate interactions, and $\Delta\sigma_{ds}$ is the contribution from dislocation-solute interactions. It is this last stress contribution, $\Delta\sigma_{ds}$, which encompasses the DSA effects and becomes of great importance within the DSA region.

One of the more important manifestations of DSA is negative strain rate sensitivity (SRS). In a normal deformation process, as the strain rate is decreased, the material's flow stress will also decrease. This is a result of the decrease in dislocation velocity, which results in decreased resistance to motion. Within the DSA region, the opposite holds true. In other words, the flow stress will decrease as the strain rate is increased. This is due to the longer time dislocations spend arrested at obstacles while travelling at the lower velocity. More solute atoms are able to diffuse to the dislocations, thereby increasing the strengthening effect and requiring higher stresses to move these dislocations.

The effect of negative SRS on the stress versus temperature curves of a material is illustrated in **Figure 2.8**. This figure depicts the flow stress of two different materials as they vary with temperature. The dashed lines represent a pure material with no signs of DSA while the solid lines represent an alloyed material exhibiting DSA. There are two curves for each material indicating a high and low strain rate. The curves for the pure material continually soften with increasing temperature and, as expected, an increase in strain rate results in an increased flow stress. This is not true for the alloyed material.

This material features a prominent hump on both curves resulting from the presence of DSA. It can also be seen that an increase in the strain rate shifts the hump to higher temperatures. The phenomenon known as negative SRS occurs within *region b*. It can be seen that by increasing the strain rate, there is actually a drop in the flow stress of the alloyed material. Conversely, in *region c*, when going from a low strain rate to a high strain rate, an abnormally high increase in the flow stress is observed.

The practical significance of having a negative strain rate sensitivity is that deformation becomes *easier* at higher strain rates. This, in turn, can lead to flow localization and then the presence of shear bands. Such microstructural features affect the annealed texture in steels and can also lead to catastrophic low-strain failure³⁵.

Another interpretation regarding negative SRS was proposed by Baird and Jamieson³⁶. They suggested that negative SRS resulted from the localized exhaustion of sufficient solute atoms to pin the dislocations. The material is weaker in these solute-depleted regions and, hence, will preferentially deform in these areas.

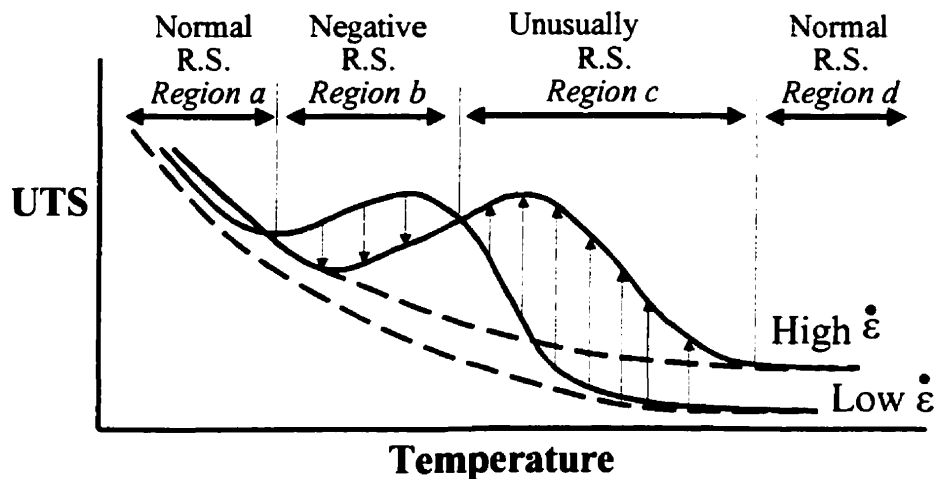


Figure 2.8: Stress versus temperature curves showing a comparison of materials that do and do not exhibit DSA³⁵.

2.3 THE EFFECT OF CHEMICAL COMPOSITION ON STRAIN AGING

Two types of alloying elements can be distinguished in connection with strain aging, both static and dynamic, in steel. The first class is composed of elements that are directly responsible for strain aging. These elements possess enough mobility to keep up with mobile dislocations and effectively pin them. The second class of elements includes those that affect the process by altering the composition or the mobility of the solute atoms responsible for the strain aging¹¹.

The effectiveness of the first class of elements is dependent upon the following three characteristics:

- the solubility of the element in question
- its diffusion coefficient
- the severity with which it locks dislocations, i.e. its binding energy

Interstitial elements that possess these characteristics and are possible contributors to strain aging effects are carbon, nitrogen, oxygen and hydrogen. Claims regarding the effects of oxygen and hydrogen have been effectively dispatched due to the fact that these elements are too mobile at room temperature or above to lock dislocations¹¹. Carbon and nitrogen are now accepted as the primary causes of strain aging effects in steel. Nitrogen is believed to have the more profound effect. This is a result of its higher solubility and diffusion coefficient as well as its high binding energy.

The second class of elements can be divided into four categories based upon their interactions with carbon and nitrogen:

- elements that interact weakly or not at all with C and N – Cu, Ni, Mn, P;
- the nitride formers – Al, Si, B;
- the carbide formers – Mo;
- the carbonitride formers – Cr, V, Nb, Ti.

Generally, elements such as copper and nickel that do not interact appreciably with either carbon or nitrogen are thought to increase the propensity for strain aging slightly. This may indicate that these elements increase the solubility of carbon and nitrogen. Manganese and phosphorus, which attract nitrogen, probably retard strain aging¹¹.

Carbide formers as well as nitride formers decrease strain aging effects by removing the selected element, carbon or nitrogen, from solution thereby providing less solute atoms to lock the dislocations. Elements that form carbonitrides (chromium, vanadium, niobium and titanium) can eliminate strain aging if present in sufficient quantities; the initial yield point is also eliminated. If an insufficient quantity is present, the strain aging contribution of nitrogen will be eliminated first. This is due to the fact that these elements have a higher affinity for nitrogen. The effectiveness of these elements in preventing strain aging increases in the order of their affinity for carbon and nitrogen as follows: Mn, Cr, V, Nb, Ti.

2.4 PRACTICAL IMPLICATIONS OF STRAIN AGING

From a practical standpoint, it is important to eliminate strain aging effects because they can lead to problems during forming operations. Strain aging can affect cold forming operations by reducing the material's ductility or modifying its toughness during cold working. In fact, some researchers have reported head bursts, shear cracking and increased wear of tools in steel due to the occurrence of dynamic strain aging during the production of fasteners by cold heading operations³⁷.

Another processing problem is the appearance of surface markings or "stretcher strains" during deep-drawing operations⁷, as seen in **Figure 2.9**, due to localized heterogeneous deformation. The localized deformation is a result of the negative work hardening associated with the occurrence of yield drops, i.e. with SSA. This localized flow was also noted in the wire drawing of steel. DSA was cited as the reason for the wire breaks that were not related to the presence of large inclusions, rolling defects or improper drawing machine setup²². Furthermore, during industrial wire drawing, if aging can take place as a result of deformation heating during processing, multi-stage strain aging will significantly reduce the ductility, leading to wire breaks³⁸.

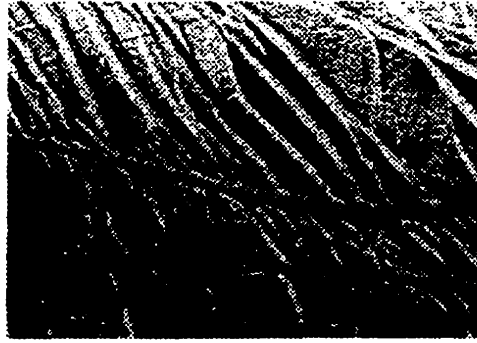


Figure 2.9: Stretcher strains on a steel sheet stretched past the yield point³⁹.

Therefore, the operating conditions (i.e. temperature and strain rate) must be carefully considered during forming operations to avoid the effects of static and dynamic strain aging. As has been previously stated, strain aging (both SSA and DSA) is dependent upon the solute content and solubility of an alloying element or an impurity. Thus, by carefully monitoring the solute content of these elements during processing, one can greatly reduce the effects of strain aging. For example, any pre-treatment that increases the amount of the element in solution will increase a material's susceptibility to strain aging.

However, the effects of strain aging are not wholly negative. Strain aging can also be used positively as a strengthening mechanism. For example, bake hardening uses the strengthening effect of static strain aging during heating after painting to improve the mechanical properties of a material. It involves heating a preformed material to allow the diffusion of the solute atoms in solution to dislocations, thereby pinning them and strengthening the material. DSA can also be used as a prior thermomechanical treatment to improve the room temperature strength. Also, DSA at moderately high temperatures can serve as a strengthener by increasing the work hardening rate; in this way, it can also improve a material's fatigue and creep strength²⁰.

2.5 CONTROLLING STRAIN AGING

Numerous solutions to control the occurrence of strain aging have been developed, some of which will be briefly discussed in this section. One method of

removing the effects of strain aging is to temper roll or roller level the sheet prior to subsequent deformation by drawing. These methods induce a strain so as to unpin any locked dislocations. This then removes the yield point provided the material is not allowed to age once more. In the case of temper rolling, a light reduction is used to improve the material's ductility¹⁰. The drawback to this method is its installation costs, which are quite high. Roller levelling is much less expensive; however, it is less effective in removing yield point elongation¹¹.

Another method that can be used to eliminate static strain aging is to store the material below room temperature. By doing this, the aging process is slowed down since diffusion is a temperature dependent process. When stored, the material is at temperatures of 0°C or below, where the rate of aging is negligibly low. Once again, this method requires high capital expenditures.

Perhaps the most effective way to prevent the static and dynamic strain aging caused by interstitial solutes is to add microalloying elements; these then form carbides, nitrides, or both. There are various types of elements that fall into these categories, as was seen previously. In any case, these elements are effective in removing the carbon and/or nitrogen from solution (i.e. in "fixing" the C and N). By doing so, there is less solute available to interact with the dislocations. Therefore, the material's susceptibility to strain aging is reduced. The effectiveness of this method depends on the extent to which the solute atoms responsible for strain aging are removed from solution. One possible drawback is that the addition of these alloying elements in sufficient quantities to eliminate strain aging may not be desirable. Such additions could lead to new problems or be too expensive to be considered cost effective.

2.6 STRAIN AGING CAUSED BY SUBSTITUTIONAL ELEMENTS IN STEEL

Most of the previous work on strain aging, whether it is static or dynamic, has focused on the effects of the interstitial rather than substitutional elements. Some work has been conducted on the DSA caused by substitutional elements, although most of it

has concentrated on FCC materials such as aluminum or the HCP zinc alloys. There has been very little research conducted on the SSA or DSA of steel at higher temperatures.

As has been outlined through the majority of this literature review, strain aging resulting from interstitial elements takes place at relatively low temperatures ranging from approximately 100 to 300°C (i.e. within the blue brittle region). In this region, the diffusion rates of the interstitial elements are many orders of magnitude higher than of the substitutional elements. In order for the substitutional elements to produce the same effects, the temperature range must therefore be significantly higher. That is to say, a temperature range must be chosen wherein the diffusion rates of the substitutional elements are comparable to the travelling velocities of the dislocations. A comparison of the diffusion coefficients of interstitial and substitutional elements in steel is presented in **Figure 2.10**. Assuming that the diffusion coefficients for the substitutional elements must equal those for carbon and nitrogen (in the blue brittle region) for any type of strain aging to occur, the temperature range is found to be 900 to 1350°C, depending on the substitutional element of interest. From **Figure 2.10**, it can also be seen that carbon, nitrogen and sulfur diffuse too rapidly to produce any strain aging effects within that temperature range.

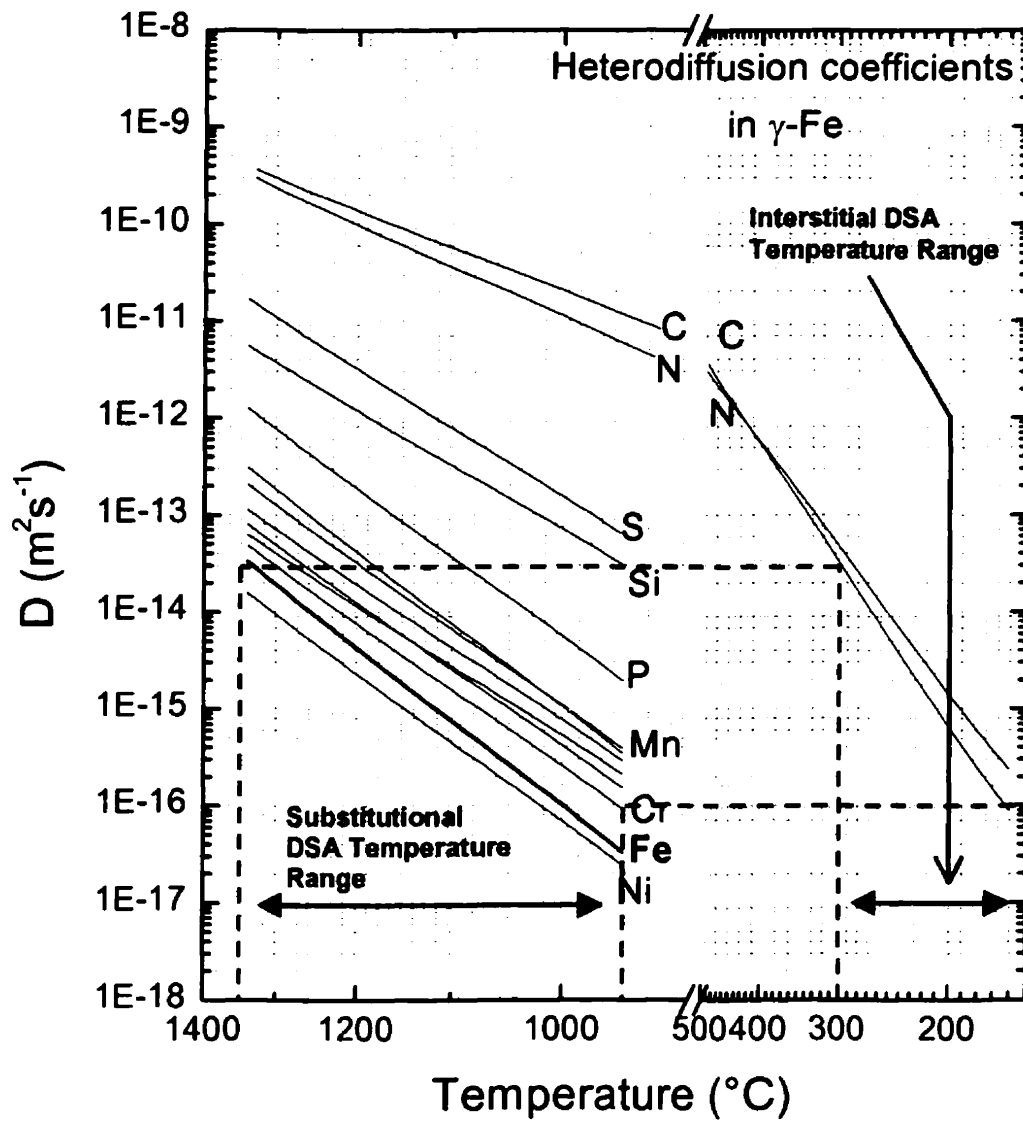


Figure 2.10: Diffusion coefficients of the interstitial and substitutional elements in iron⁴⁰.

2.7 SUMMARY

Strain aging can occur *during* or *after* deformation. Aging during deformation is termed dynamic strain aging. It results from the continuous pinning and unpinning of dislocations by solute atoms while the material is being strained. Hence, it occurs when solute atoms gain enough mobility to keep up with moving dislocations and hinder their motion. Strain aging following deformation is known as static strain aging. It results from the locking of dislocations by solute atmospheres. The elements responsible for strain aging effects can be interstitial or substitutional, depending on the temperature, time and strain rate.

Much of the work by previous investigators has concentrated on the effects of the interstitial elements at low temperatures (100 to 300°C). Little or no research has been conducted on the effects of the substitutional elements in steel at high temperatures. It was to fill this gap that the research described below was undertaken.

CHAPTER 3

EXPERIMENTAL DETAILS

This chapter outlines the testing methodology followed throughout the course of the research. A description of the material, testing apparatus, testing method and the types of tests conducted is contained within the following sections.

3.1 MATERIALS

There were two types of steels used in these experiments. The chemical compositions of the two steels are listed in **Table 3.1** below.

Table 3.1: Chemical compositions of the experimental steels in wt%

Steel	Cr	Ni	C	P	S	Si	Cu	Mn	Nb	Ti
Typical 304	18-20	8-10.5	0.08	0.045	0.03	1.00	--	2.00	--	--
A	18.41	8.21	0.072	0.027	<0.003	0.57	0.41	1.08	0.031	0.033
B	18	12	All other elements < 15 ppm							

--" Indicates not listed

Steel A is a type 304 stainless steel obtained from Atlas Stainless Steel in Tracy, Quebec. As seen in **Table 3.1**, where the chemical composition of Steel A is compared to that of a typical 304 stainless steel, it is well within specifications. Steel A was used for the majority of the experiments at various temperatures and strain rates.

Steel B is composed primarily of chromium (Cr) and nickel (Ni). All the other elements (both the alloying and impurity elements) had a combined wt% below 15 ppm. This steel was used in order to determine whether Cr and/or Ni were responsible for the static and dynamic strain aging effects observed when testing steel A.

3.2 UNIAXIAL COMPRESSION TEST

The compression test was used as the standard method of experimentation. This method was employed as opposed to the previous investigator's testing method of torsion testing³⁵. The advantage of compression testing over torsion testing is that deformation throughout the sample is more uniform. Compression testing can also allow for high strain rate testing, although this was not possible in the present case⁴¹.

3.2.1 SPECIMEN PREPARATION

The stainless steel received from Atlas Stainless Steel was in the form of a billet approximately 30 cm x 15 cm x 15 cm. The billets were sectioned and then machined into cylindrical compression specimens with their longitudinal axes parallel to the rolling direction. The specimen height was 11.41 mm and the diameter was 7 mm. These dimensions were chosen in order to promote homogeneous deformation. It has been shown that there exists a practical limit of $D_o/h_o \approx 0.5$ ⁷. Below this value, the specimen buckles rather than barrels, providing inhomogeneous deformation.

Another method of ensuring homogeneous deformation is by reducing friction between the specimen and the tools. This was accomplished by inserting a thin sheet of mica between the specimen and the tools, both at the top and the bottom. Mica serves as a lubricant, thereby decreasing friction.

3.2.2 COMPRESSION TESTING SYSTEM

The compression tests were carried out on a Material Testing System (MTS) Model 510 machine. The MTS is composed of a load frame rated for a maximum load of 25 kN, a hydraulic power supply and a closed loop servohydraulic and computerized outer loop system. There is also a hydraulic actuator controlled by a servovalve that generates the force and linear displacement. The force exerted on the specimen is measured through a load cell, while a Linear Variable Differential Transformer (LVDT) measures the displacement. The system is controlled by, and was interfaced with the servohydraulics through, a 486 microprocessing unit. The control system is basically responsible for command generation, data acquisition and real-time decision making. The compression tests were executed using software programs written in the MTS BASIC computer language. A schematic of the compression testing machine is shown in **Figure 3.1**.

3.2.3 COMPRESSION TOOLS

The compression tests performed in this experiment were all carried out at high temperatures. The compression anvils and the specimen are exposed to high temperatures during each test. Therefore, the material used for the anvils must be able to withstand the high temperatures and flow stresses associated with these experiments. The compression anvils are fabricated of an alloy named TZM. TZM is a molybdenum-base alloy containing a dispersion of 0.5% Ti and 0.08% Zr oxides. The oxides improve the high temperature strength of the alloy. The alloy also possesses good creep resistance and a high melting point, which makes it a suitable material for these experiments.

3.2.4 FURNACE AND TEMPERATURE CONTROL

To perform the high temperature compression tests, a radiant furnace manufactured by Research Inc. with a 16 kW power supply was used. The furnace was attached to the columns of the MTS load frame. The furnace is composed of four tungsten filament lamps and four mirror finished elliptical reflectors of aluminum. The heat generated by the four lamps is reflected to the center of the furnace by the four aluminum reflectors. The temperature is measured using a K-type Chromel-Alumel

closed-tip thermocouple in contact with the specimen. The furnace was linked to a Micristar controller/programmer. To prevent oxidation of the compression tools and specimen, the experiment was carried out within a sealed quartz tube in which a high purity argon atmosphere was maintained.

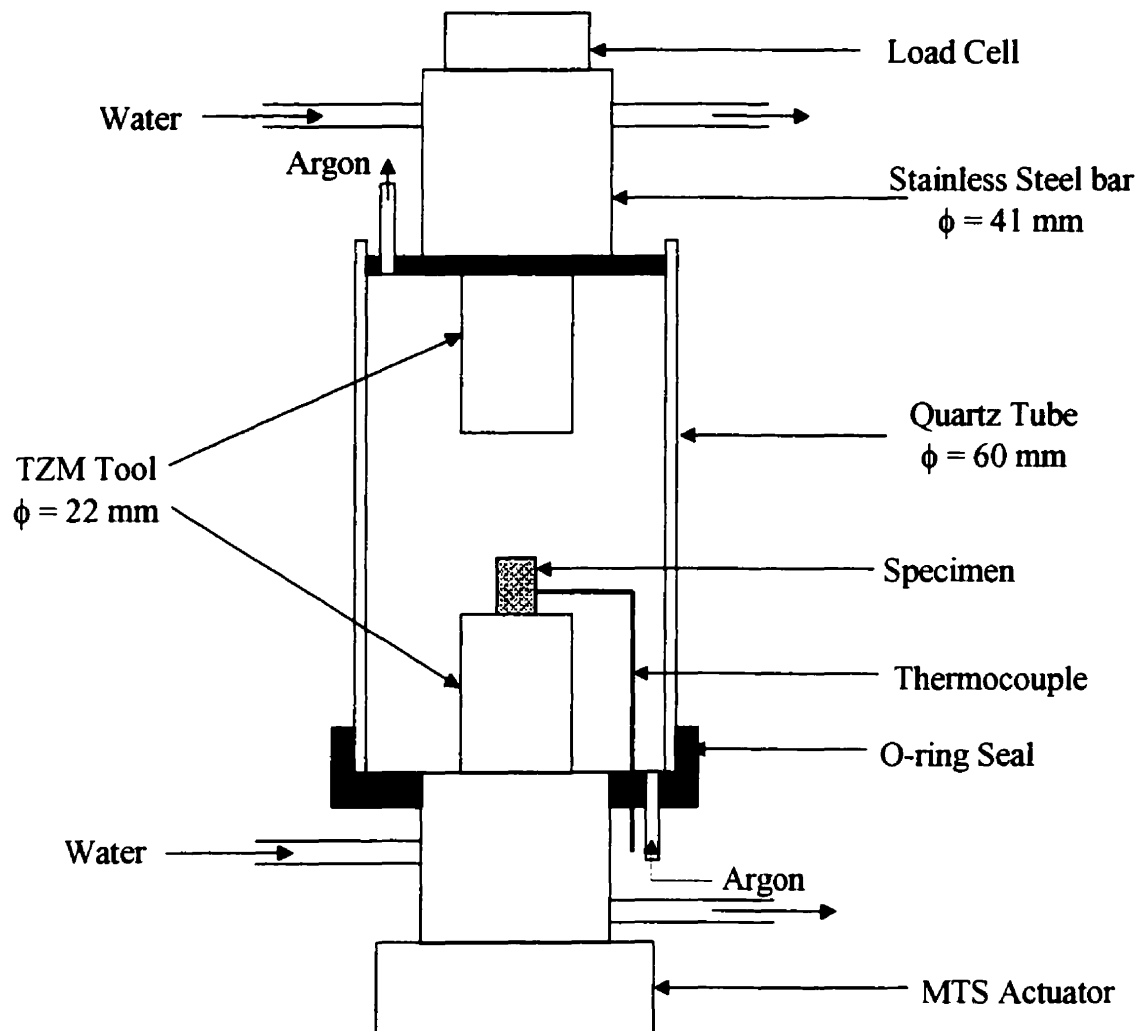


Figure 3.1: Schematic diagram of the compression testing machine⁴².

3.3 DATA ACQUISITION AND PROCESSING

Data acquisition during the experiment was conducted using the TestWare-SX software package operating under an Operating System 2 (OS/2) platform using a 486 microprocessing computer. The TestStar program allows for the programming of the deformation schedule (i.e. strain, strain rate, time) as a test template. The test templates are stored within the TestWare-SX program in Save File Playback (i.e. an *.sfp extension) file format. In addition, the program also controls data acquisition, allowing for acquisition rates of up to 1000 data points/second. The TestStar software allows one to view real-time values of the temperature, displacement and load. These values are also recorded and saved in data files for further analysis.

To facilitate data analysis and manipulation, the TestStar data files were converted into spreadsheet files. Conversion and interpretation of the experimental data were conducted using two types of spreadsheet software, Microsoft EXCEL and Microcal ORIGIN. These are similar software packages, although ORIGIN allows for data manipulation beyond the capabilities of EXCEL.

The load-displacement data contained within the data files were converted into values of stress and strain. Stress-strain curves were then plotted to graphically express the experimental data and facilitate analysis. The following equations were used in the conversion process:

$$D_0^2 h_0 = D^2 h \quad (3.1)$$

$$\sigma = \frac{4P}{\pi D^2} \quad (3.2)$$

$$\sigma = \frac{4Ph}{\pi D_0^2 h_0} \quad (3.3)$$

$$\epsilon = \ln \frac{h_0}{h} \quad (3.4)$$

Equation 3.4 represents the constancy of volume of the specimen throughout the experiment, where D_0 and h_0 are the initial diameter and height and h is the height of the

cylindrical specimen at any instant during compression. P is the load or force applied to the specimen during the compression test. Here, the usual convention that the stress and strain are both negative during compression was not employed.

3.4 THERMOMECHANICAL PROCESSING (TMP) SCHEDULE

All the experiments followed a similar thermomechanical processing (TMP) schedule. A schematic of the TMP schedule can be seen in **Figure 3.2**. The specimen was first heated to the test temperature and then held there for 15 minutes. This step was conducted to ensure that there was no temperature gradient present within the sample. The specimen was then tested under various conditions, which will be described in the subsequent section. Once the test was done, the specimen was allowed to cool to room temperature.

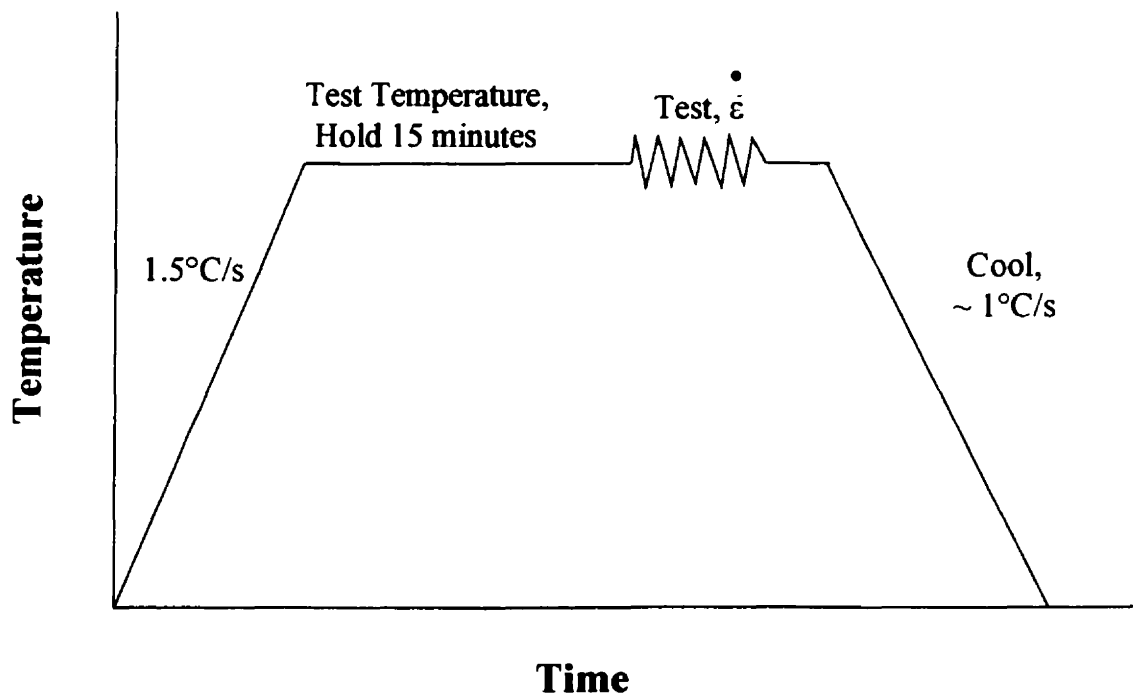


Figure 3.2: Schematic diagram of the TMP schedule employed.

3.5 TYPES OF TESTS

There were two types of tests that were performed in order to determine the range over which static and dynamic strain aging occurred as a result of the presence of substitutional elements. All the tests were configured so that they could be performed in compression, since this was determined to be the most effective test for gathering evidence of both SSA and DSA.

The first set of experiments consisted of simple compression tests at constant strain rate. Strain rate change tests served as the second type of experiment and were conducted in order to search for further evidence to support the conclusion that DSA was occurring within the test temperature regime. These testing techniques are further described in the following sections.

3.5.1 SIMPLE COMPRESSION TESTS

The simple compression test involved deforming the specimen in compression at a constant strain rate to a specified strain. The experiments were performed in multiple passes, meaning that the specimen was strained, unloaded for a period of time, and then strained again. In certain cases, the specimen was unloaded more than once. However, most experiments consisted of only two passes. This type of testing allows one to vary the strain applied per pass. The pass strains examined in this experiment ranged from 0.1 to 0.4. The test temperatures ranged between 800 and 1200°C, in 50°C increments, while strain rates of 0.01, 0.5, 1 and 5 s⁻¹ were investigated. The interruption or interpass times ranged from as low as 0.01 s to as high as 50 s.

This type of testing was performed on both steel A and steel B. Steel A was used to determine the domain within which SSA and DSA appeared. Steel B was used much more sparingly due to the limited number of specimens available. Therefore, only regions that exhibited strong evidence of SSA and DSA were examined. This included a strain rate of 0.5 s⁻¹ and temperatures of 1000 and 1100°C.

3.5.2 STRAIN RATE CHANGE TESTS

The strain rate change tests involve changing the strain rate during deformation and observing the material's response. In a normal thermally activated process, the response to an increase in the strain rate would be an increase in the flow stress. However, within the DSA domain, an increase in strain rate could be expected to result in a *decrease* in the flow stress, as described in the previous chapter. Therefore, these tests were carried out using steel A in order to provide further evidence that DSA is occurring.

A schematic of the deformation cycle can be seen in **Figure 3.3**. The test basically involved straining the specimen to a strain of about 0.2 and then increasing the strain rate. Then another strain of 0.2 was applied and the strain rate was decreased to its original value once more.

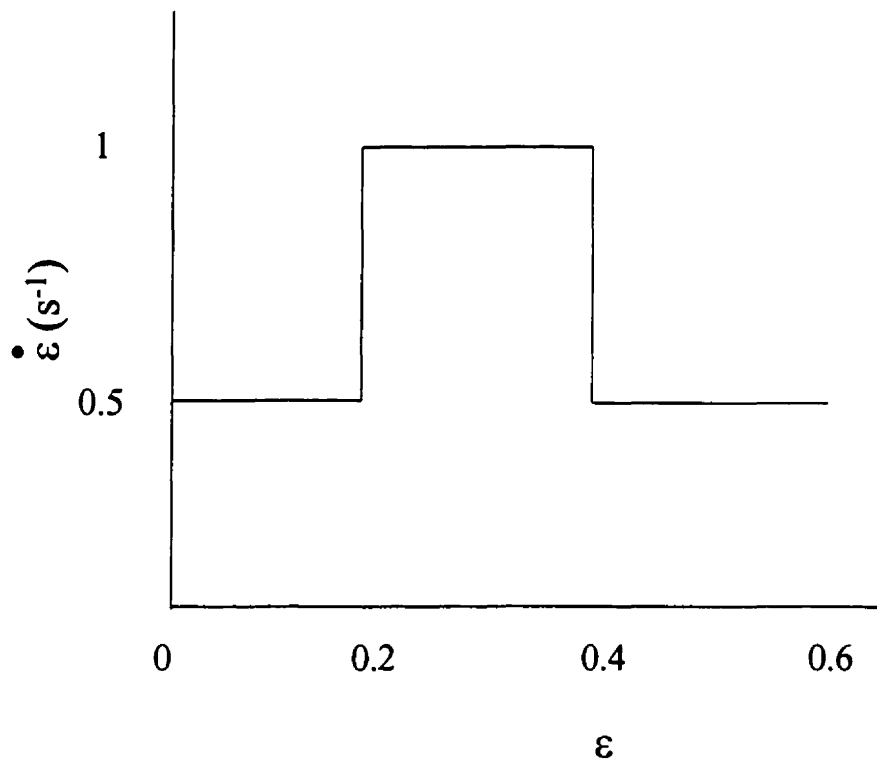


Figure 3.3: Schematic diagram of the deformation cycle employed during the strain rate change tests.

CHAPTER 4

RESULTS AND DISCUSSION

This chapter presents data (both graphical and numerical) obtained from the various experiments described in **Chapter 3**. The results are presented and then described based purely on the experimental data obtained from the tests. The author then explains the possible causes of the phenomena observed throughout the experiments.

4.1 SIMPLE COMPRESSION RESULTS FOR STEEL A

This section presents the results obtained from the first set of experiments performed in simple compression as outlined in the previous chapter. These experiments were conducted on both steels A and B and are therefore presented in two sections. Steel A was a typical stainless steel. Its chemical composition is listed in **Table 3.1**. The stress-strain curves for steel A were determined over the temperature range 800 to 1200°C at a strain rate of 0.5 s^{-1} . In these tests, the effects of temperature, pass strain and interpass (interruption) time on the characteristics of static and dynamic strain aging were investigated. In certain cases, the effect of strain rate was also investigated. **Figures 4.1 to 4.3** illustrate the general appearance of the flow curves over that temperature range.

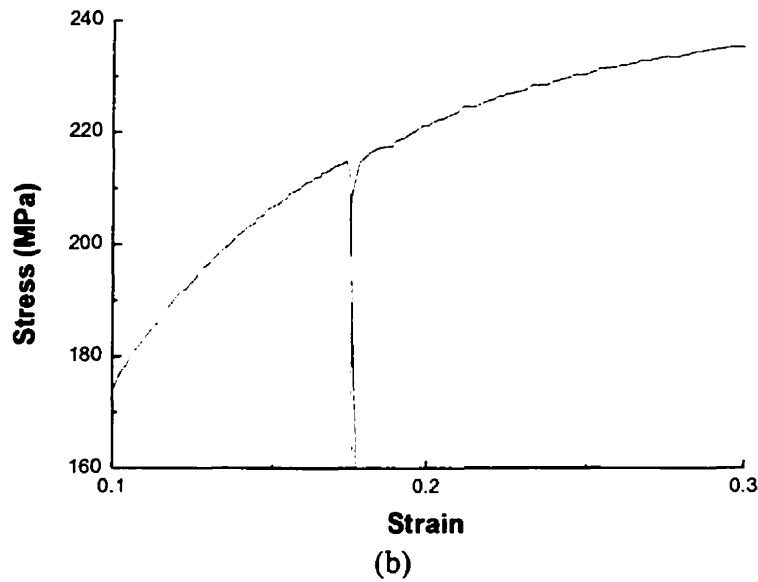
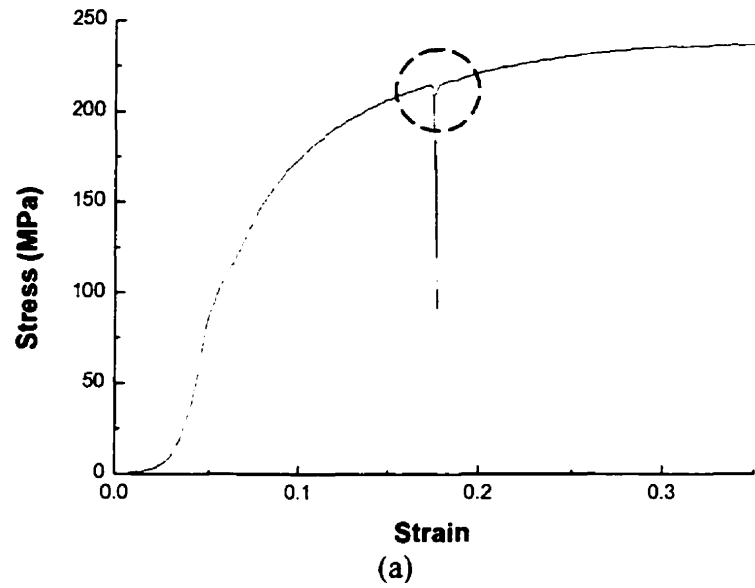


Figure 4.1: (a) Stress-strain curve at 800°C, for a pass strain of 0.2, an interpass time of 0.01 s and a strain rate of 0.5 s⁻¹; (b) magnification of the circled region.

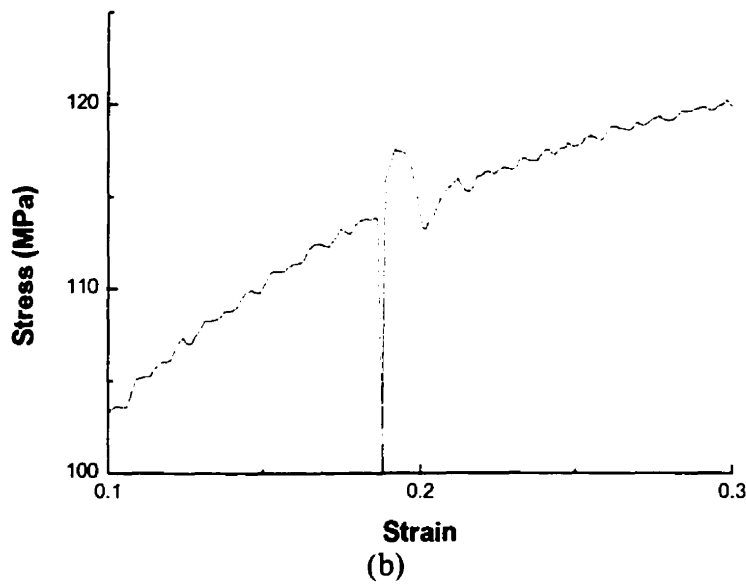
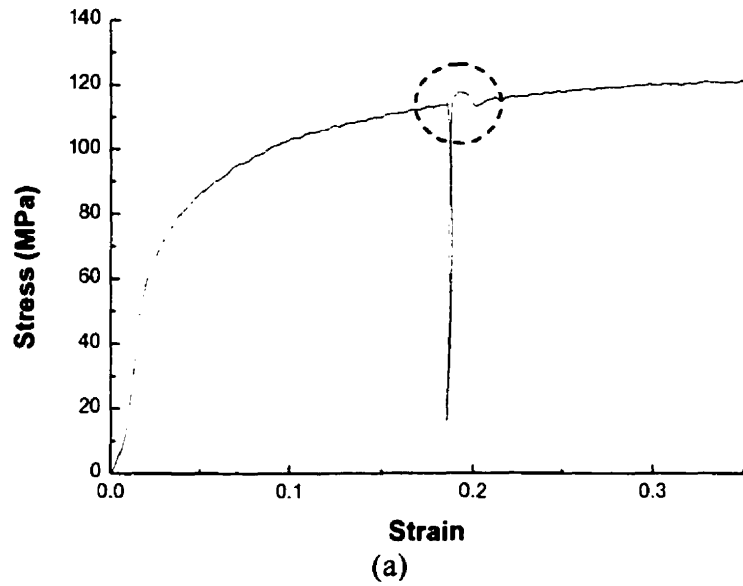


Figure 4.2: (a) Stress-strain curve at 1000°C, for a pass strain of 0.2, an interpass time of 0.01 s and a strain rate of 0.5 s^{-1} ; (b) magnification of the circled region.

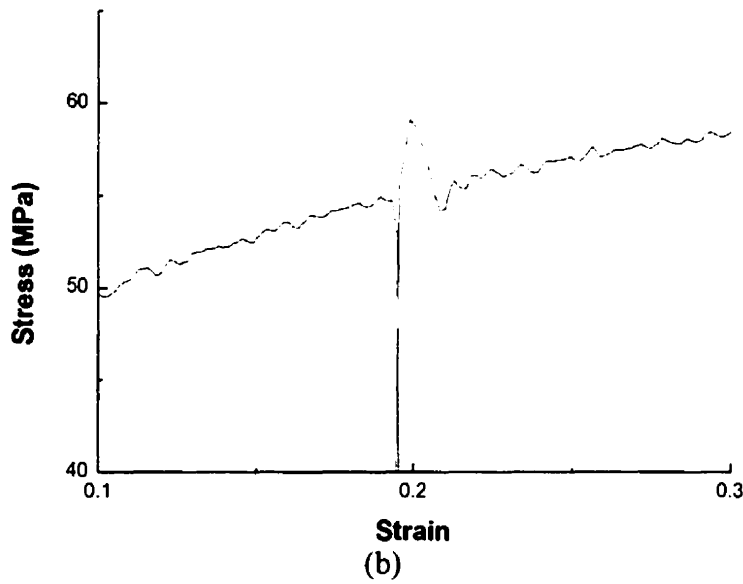
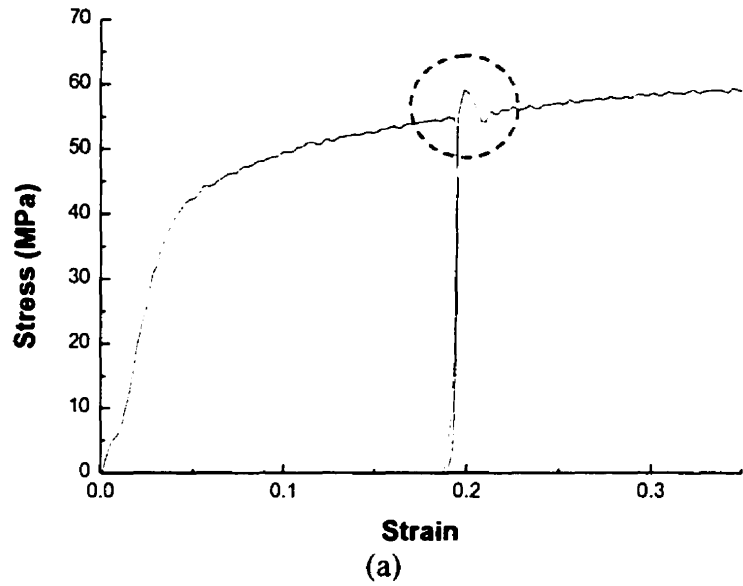


Figure 4.3: (a) Stress-strain curve at 1200°C, for a pass strain of 0.2, an interpass time of 0.01 s and a strain rate of 0.5 s^{-1} ; (b) magnification of the circled region.

It can be seen from **Figures 4.1 to 4.3** that the steel A flow curves depend on temperature. As expected, the flow stress of the material changes significantly with temperature. It is known that, as the temperature is increased, a metal flows more easily (i.e. the flow stress decreases); therefore, it is easier to deform. The highest flow stress was observed at a temperature of 800°C, while the lowest flow stress was found at 1200°C. The flow stress at 1000°C had an intermediate value.

It is important to note the significant differences between the 800°C flow curve and those at the higher temperatures. In addition to having the highest flow stress, the flow curves at 800°C exhibited no sign of either static or dynamic strain aging. After unloading the specimen for 0.01 s, there is no evidence of an SSA peak or yield drop. By contrast, when testing was carried out at temperatures of 1000 and 1200°C (**Figures 4.2 and 4.3**, respectively), yield drops attributed to SSA are clearly visible. This suggests that, at a strain rate of 0.5 s^{-1} SSA yield drops only begin to appear at some temperature between 800 and 1000°C.

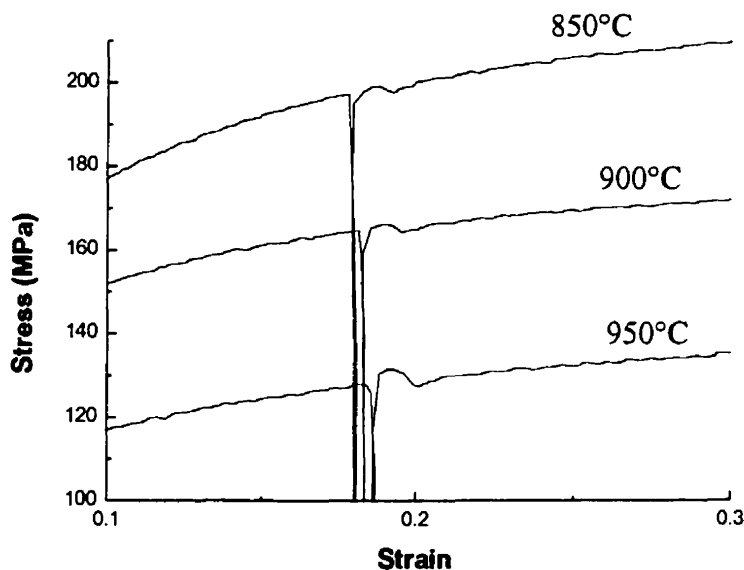


Figure 4.4: Stress-strain curves at 850, 900 and 950°C showing the appearance of serrations.

The stress-strain curves determined at intermediate temperatures of 850, 900 and 950°C are depicted in **Figure 4.4**. It can be seen from this figure that a slight peak becomes visible at a temperature of 850°C. Therefore, at some temperature between 800 and 850°C (probably closer to 850°C), SSA peaks begin to appear at a strain rate of 0.5 s⁻¹. That temperature can be said to be the lower temperature limit for the appearance of the yield drop at that strain rate.

As seen in **Figure 4.3**, the yield drops are still quite visible at a temperature of 1200°C. Unfortunately, tests above this temperature were not conducted due to the limitations of the compression testing equipment, which was not designed to operate above 1200°C. Therefore no upper limit was established in these tests. However, it is likely that as the temperature is increased, the SSA peaks will eventually disappear. This would then create temperature limits for the appearance and disappearance of SSA yield drops at a given strain rate, similar to the appearance and disappearance of the serrations seen in **Figure 1.4**.

The effect of temperature on the visual appearance of the SSA yield drops is also evident when examining **Figure 4.4**. As the temperature is increased from 850 to 950°C, the size of the yield drop can be seen to increase. This is also seen when comparing the flow curves at 1000 and 1200°C, **Figures 4.2a** and **4.3a** respectively. It should also be noted that the “yield drops” are not as sharp at these elevated temperatures as they are in the vicinity of room temperature.

Dynamic strain aging serrations are also absent on the steel A flow curve at 800°C. However, as was the case with the SSA peaks, slight serrations become visible at 850°C. Once again, the lower temperature limit for the appearance of DSA serrations can be said to lie at some temperature between 800 and 850°C. It was concluded that these serrations are attributable to DSA as a result of the substitutional elements present. The severity of the serrations increases with increasing temperature. Although there is not much difference between the serrations at 850 and 950°C, there is a noticeable difference

in the appearance of the serrations at 850°C and those present at temperatures of 1000 and 1200°C.

It should be noted that the serrations visible at temperatures ranging from 850 to 1200°C might not be attributable solely to DSA. The presence of machine noise must also be considered. However, since the severity of the serrations increases and becomes quite pronounced at temperatures above 1000°C, it can be concluded that DSA is at least in part (if not fully) responsible for the appearance of these serrations.

There also appears to be a particular strain required for the appearance of serrations. As discussed in **Chapter 2**, this can be termed the “critical strain”. This is most easily identified when examining **Figure 4.3a**. Beginning at zero, the flow stress increases in a smooth fashion until it reaches a strain of approximately 0.05. Once a strain of 0.05 is surpassed, the serrations become visible and continue until the specimen is unloaded. Once deformation is resumed after the unloaded interval, the yield drop is noticed followed by the reappearance of the serrations. The presence of the critical strain suggests that certain concentrations of vacancies and dislocations are required to produce the serrations observed. This makes sense in that an increased concentration of deformation vacancies will increase the diffusion rate of substitutional atoms. This interpretation will be discussed in more detail in a subsequent section. On the other hand, an increase in the dislocation density will increase the number of dislocations per unit area, facilitating dislocation pinning by solute atoms in this way.

4.1.1 THE EFFECT OF PASS STRAIN

The “pass” strain is basically the strain applied to the specimen per deformation cycle. It represents the reduction that could be applied in a rolling mill during a specific pass. Experimentally, it is the strain applied to the specimen before it is unloaded. **Figures 4.1 to 4.4** depicted compression tests conducted using an applied pass strain of 0.2. To observe the effects of varying the pass strain on the presence of SSA and DSA, simple compression tests were also conducted using pass strains of 0.1 and 0.4. The results of these experiments can be seen in **Figures 4.5 and 4.6**.

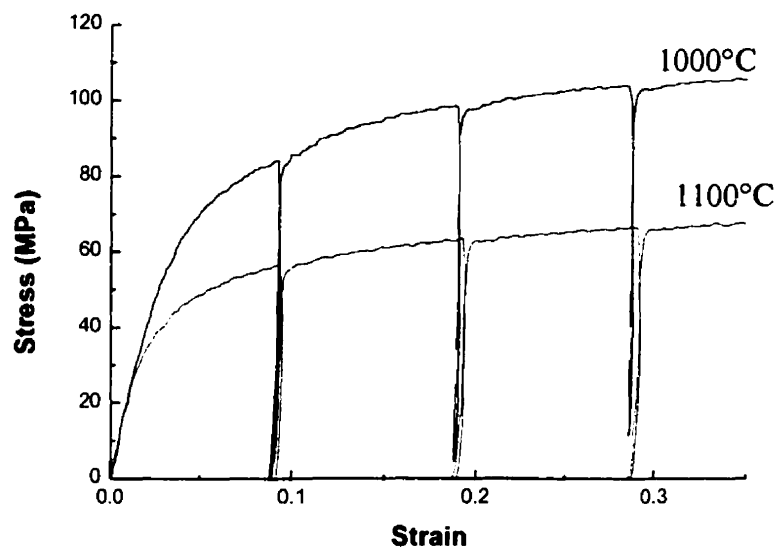


Figure 4.5: Stress-strain curves obtained using a pass strain of 0.1; strain rate = 0.5 s^{-1} ; interpass times = 0.01 s.

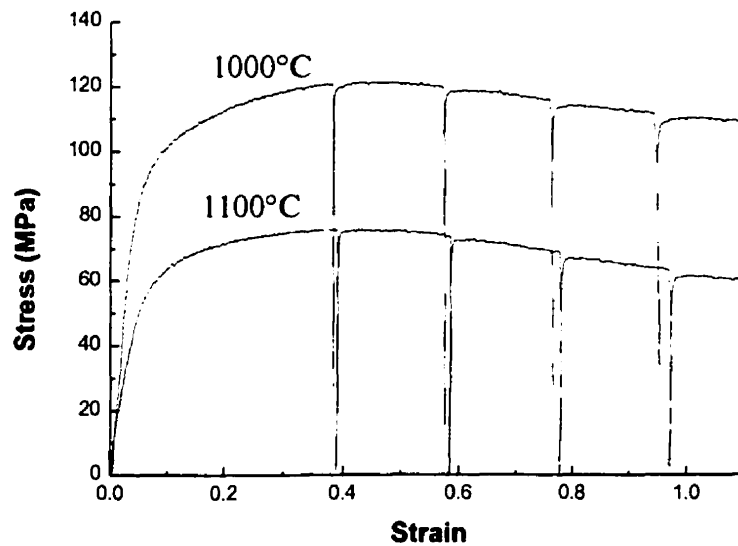


Figure 4.6: Stress-strain curves obtained using a pass strain of 0.4; strain rate = 0.5 s^{-1} ; interpass times = 0.01 s.

The data obtained from multi-pass compression tests using a pass strain of 0.1 are illustrated in **Figure 4.5**. These tests were conducted at temperatures of 1000 and 1100°C. It is clearly evident that no SSA yield drops are present during any of the passes. It can also be seen that the flow stress decreases as the temperature is increased. Nevertheless, at both temperatures, the flow stress is lower than it was when using a pass strain of 0.2. This is a direct result of the reduction in work hardening that accompanies a reduced pass strain.

When the pass strain was increased from 0.2 to 0.4, shown in **Figure 4.6**, the SSA yield drops again disappeared. As before, the flow stress can be seen to decrease with an increase in temperature from 1000 to 1100°C. However, in this case, the flow stress levels are higher than those corresponding to pass strains of 0.2. This holds true at both 1000 and 1100°C.

Therefore, it appears that there is a critical strain associated with the appearance of SSA yield drops. This is similar to the critical strain that precedes the appearance of DSA serrations. However, there also appears to be an upper limit to the critical strain. Beyond this point, yield drops no longer appear. The appearance and disappearance of the yield drops resulting from changes in pass strain can be explained by considering the changes in dislocation density. By assuming the existence of a critical strain, one can also assume that there exists a critical dislocation density for the presence of SSA. This critical dislocation density is achieved by applying a pass strain of 0.2. By reducing the pass strain to 0.1 or increasing it to 0.4, the yield drops disappear, indicating that the dislocation density is either insufficient or else too high to produce SSA. An alternative explanation involves the production of a minimum concentration of deformation vacancies. If this concentration is too high, the SSA effects disappear. The effect of deformation vacancies will be examined in more detail in a subsequent section.

Since the dislocation density increases as a material is strained, by reducing the pass strain from 0.2 to 0.1, the dislocation density is thereby decreased. With regard to SSA, the result is that the dislocation density is then too low to produce any aging effects

once the material is reloaded. This also explains the increase and decrease in flow stress of the material by changing the pass strain, since increases or decreases in the strength and hardness of materials are closely associated with the dislocation density⁴³.

While the above explanation holds true for reducing the pass strain to 0.1, it does not fully explain the results obtained when the pass strain is increased to 0.4. Increasing the pass strain also increases the dislocation density. Therefore, the dislocation density should have been sufficiently high to enable SSA to take place. This was not the case. This may be explained when taking into consideration the effects of recovery and recrystallization on a metal. Both these processes result in a decrease in the concentration of dislocations and vacancies and are carried out through dislocation and grain boundary motion^{43,44}. The critical strain for dynamic recrystallization (recrystallization *during* the deformation process) is usually 0.6-0.8 times the peak strain⁴⁵. In this case, the peak strain is approximately 0.4; therefore, it can be seen that dynamic recrystallization has indeed started. The grain boundary motion associated with dynamic recrystallization may prevent the yield drops from being observed. Alternatively, this might be a consequence of the high density of deformation vacancies, a topic that has not yet been discussed in detail.

It should also be noted that employing a two-pass deformation schedule with pass strains of 0.1 (**Figure 4.5**) does not yield the same results as a single pass with a pass strain of 0.2 (**Figures 4.2 to 4.4**). Although the total strain applied is the same, $\epsilon = 0.2$, there are no yield drops observed when using two passes, each of 0.1 strain. It is possible that, because of the additional interpass time, the specimen undergoes recovery, which leads to an increased loss of the deformation vacancies.

Despite the absence of the yield drops associated with SSA, serrations are still visible on both sets of curves. This is better illustrated in **Figures 4.7 and 4.8**, in which magnified versions of the 1000°C flow curves are presented. The presence of serrations can be attributed to the pinning and unpinning of dislocations by substitutional solute atoms. This indicates that, even though the dislocation density is perhaps too low to

produce any SSA effects, there are still a sufficient number of dislocations to produce DSA effects. Comparing the serrations of **Figure 4.7** with those of **Figure 4.8**, it can be seen that the severity of the serrations increases with an increase in the pass strain. Despite the effects of static recovery and recrystallization, both the dislocation density and the concentration of deformation vacancies are still higher in the material deformed with the higher pass strain. Therefore, it is easier for solute atoms to diffuse rapidly and effectively pin the dislocations. Although not shown, the same results were observed at a temperature of 1100°C for pass strains of 0.1 and 0.4.

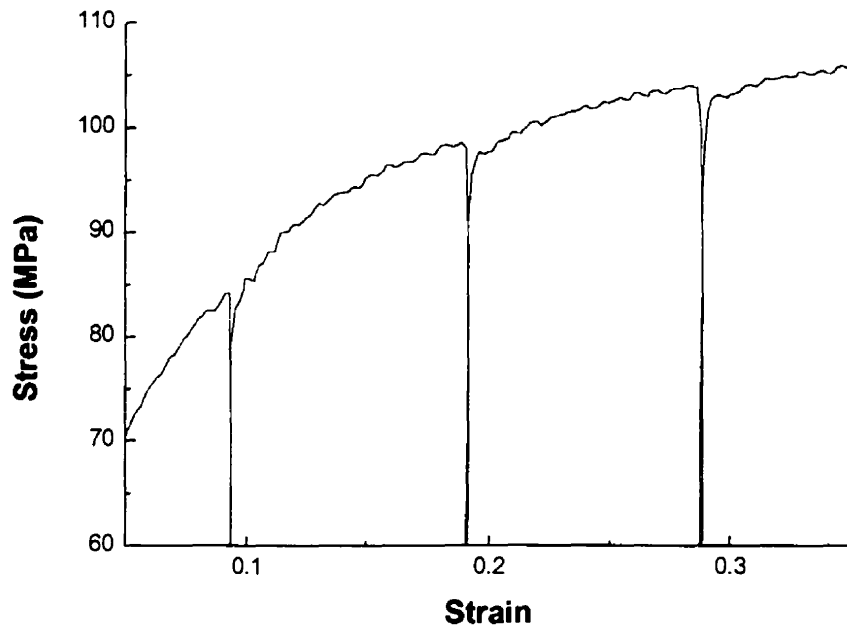


Figure 4.7: Magnified stress-strain curve determined at 1000°C using pass strains of 0.1 showing the presence of DSA serrations.

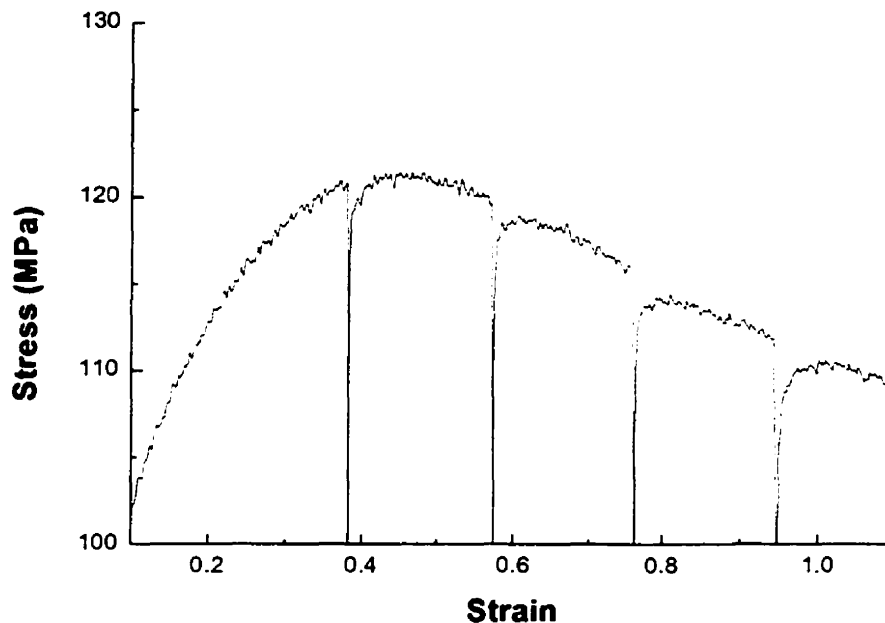


Figure 4.8: Magnified stress-strain curve determined at 1000°C using pass strains of 0.4 showing the presence of DSA serrations.

4.1.2 THE EFFECT OF INTERPASS TIME

The interpass time (also known as the interruption time) is the amount of time that elapses between deformation passes. Essentially, it is the amount of time the specimen spends unloaded. Experiments were conducted using various interpass times ranging from as short as 0.01 s to as long as 50 s. Unfortunately, due to the high data acquisition rate employed, and the limited memory capacity of the computer, tests conducted with interpass times > 50 s were not possible. The results obtained by varying the interpass times as described above are shown in **Figures 4.9 to 4.11**. These flow curves were determined at temperatures ranging from 900 to 1100°C using a strain rate of 0.5 s^{-1} and a pass strain of 0.2. It should be noted that these flow curves were magnified in order to present the corresponding data more clearly. Slight variations in the expected levels of the flow curves can also be noticed and is attributed to experimental error.

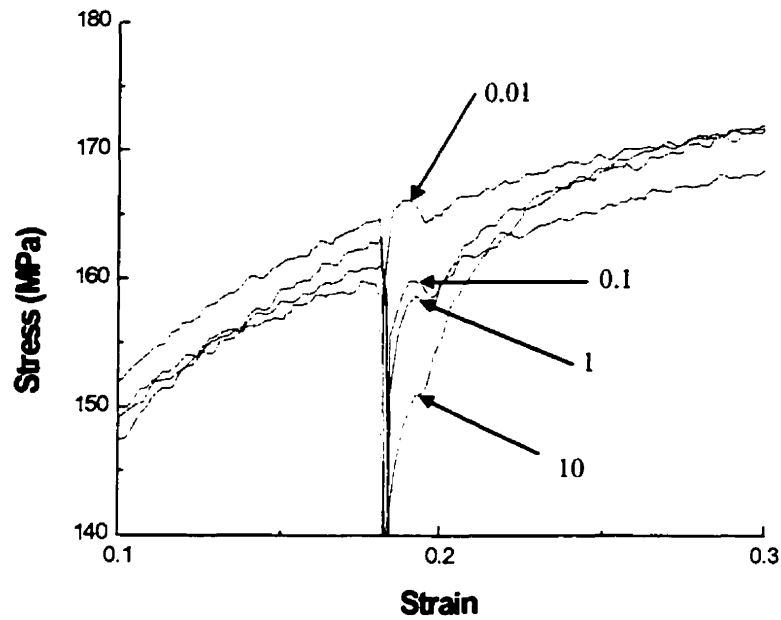


Figure 4.9: Stress-strain curves determined at 900°C and 0.5 s⁻¹ using a pass strain of 0.2. Interpass times ranging from 0.01 to 10 s were employed

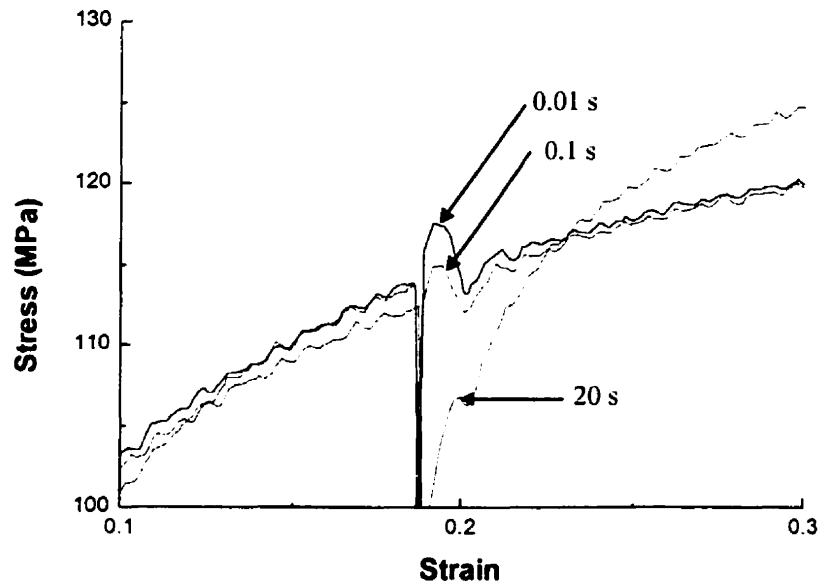


Figure 4.10: Stress-strain curves determined at 1000°C and 0.5 s⁻¹ using a pass strain of 0.2. Interpass times ranging from 0.01 to 20 s were employed.

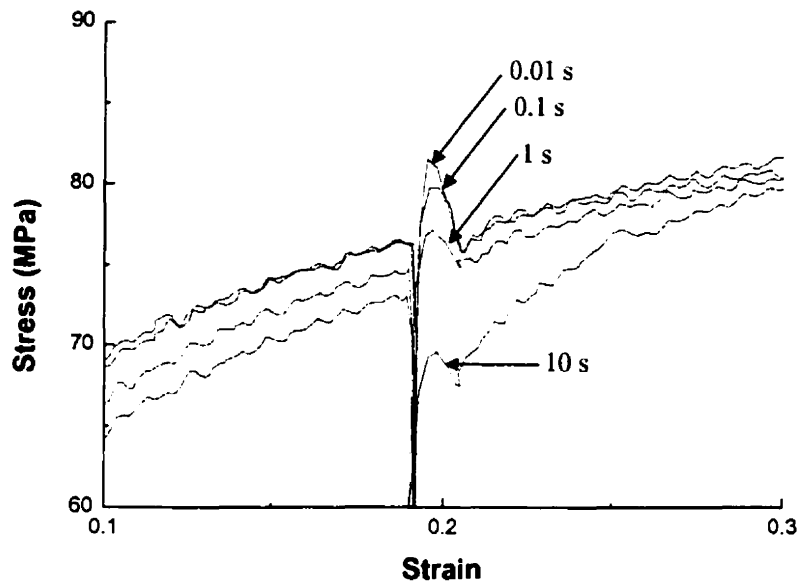


Figure 4.11: Stress-strain curves determined at 1100°C and 0.5 s^{-1} using a pass strain of 0.2. Interpass times ranging from 0.01 to 10 s were employed.

The conclusion that can be drawn by examining **Figures 4.9 to 4.11** is that, *as the interpass times increase, the SSA effects begin to disappear*. In fact, at an interpass time of 10 s at a temperature of 900°C (**Figure 4.9**), the yield drop appears to have completely disappeared. It is also evident that, as the temperature is increased, the effects take longer to dissipate. For example, at interpass times of 20 s at 1000°C and 10 s at 1100°C (**Figures 4.10 and 4.11**, respectively), the strain aging effects are still clearly visible. Although the disappearance of the static aging effects may be a simple result of “overaging”, the disappearance of these effects may be attributable to a more complex mechanism. This explanation is taken up in **Sections 4.4 and 4.5** below. At this stage, it is sufficient to say that increasing the interpass time allows for more recovery. This in turn leads to increased losses of both dislocations and deformation vacancies. As the densities of these defects decrease, so does the intensity of the yield drops until static aging effects are no longer observed. An important point to note is that the levels of the 0.1 and 1 s reloading flow curves at 1000 and 1100°C are *higher* (relative to the loading curves) than at 900°C ! This indicates that there is more short-time dislocation pinning at 1000 and 1100°C than at 900°C .

Some evidence for the occurrence of static recrystallization is provided by the amount of softening that takes place between passes. Softening is defined in terms of the decrease in yield stress upon reloading. A material that has not undergone recrystallization and therefore exhibits no softening shows no loss in strength upon reloading. Therefore, the reloading yield stress will be equal to the maximum stress prior to unloading. The degree of softening, X , taking place during the unloading period was calculated using the following expression⁴⁶:

$$X(\%) = \frac{(\sigma_m - \sigma_r)}{(\sigma_m - \sigma_o)} \times 100 \quad (4.1)$$

where σ_m is the maximum stress prior to unloading, and σ_o and σ_r are the initial and reloading yield stresses respectively. To calculate the initial and reloading yield stresses, an offset strain of 0.2% was used.

The amounts of softening taking place during the interruptions were calculated for the flow curves presented in **Figures 4.9 to 4.11**. These results are presented in **Table 4.1**. It can be seen that, for interpass times of less than one second, very little softening takes place (and less at high temperatures than at low temperatures). Typically, only a maximum of 5% softening takes place during these short intervals. The only exception was at 900°C, where 8% softening took place, but this value is only marginally higher. When the interpass times were increased by an order of magnitude (i.e. to > 10s), the amount of softening also increased dramatically. The amount of softening generally exceeded 25% in these cases.

Table 4.1: Amounts of softening (%) taking place during the interpass times.

Interpass Time (s)	900°C	1000°C	1100°C
0.01	2%	0%	0%
0.1	4%	5%	4%
1	8%	--	5%
10	32%	--	26%
20	--	27%	--

It was shown in the research carried out by Cho *et al.* that static strain aging effects disappeared when the fractional softening exceeded 30%⁴⁵. This is in agreement

with the results obtained in these experiments. At a temperature of 900°C and an interpass time of 10 s, the fractional softening was calculated to be 32%. As is evident from **Figure 4.9**, the flow curve corresponding to these parameters shows no indication of static aging. The flow curves at 1000°C and 20 s and at 1100°C and 10 s displayed softening values of approximately 27% and 26%, respectively. It can be seen that the SSA effects have noticeably diminished after these holding times. In fact, the SSA yield drop is almost gone at 1000°C at an interpass time of 20 s. Therefore, according to the results derived from these experiments and the work of Cho *et al.*, the softening values can be divided into two distinct ranges. At low softening values ($X < 30\%$), only dynamic recovery has occurred. This results in only a partial loss of dislocations so that SSA is still possible. However, high softening values ($X > 30\%$) are associated with partial to complete static recrystallization. This is accompanied by a significant decrease in the dislocation density. Hence, not enough dislocations are present to provide for any static aging effects and the yield drops disappear completely.

It is also important to note the relatively small amounts of softening taking place at the higher temperatures, namely 1000 and 1100°C. It is known that recovery is a thermally activated process. Therefore, increasing the temperature should result in increased recovery. This was not the case. In fact, it can be seen that there is less softening at 1100°C than at 900°C despite a temperature increase of 200°C. This indicates that the dislocations are pinned by solute atoms. As previously stated, the recovery process requires dislocation motion. However, if the dislocations are pinned, no recovery is possible. It was also noted that the effects dissipate with time. This is related to the deformation vacancy concentration. As the interruption time is increased, more vacancies are lost. Thus, less solute atoms are able to diffuse to the dislocations and effectively pin them. Eventually, the concentration of deformation vacancies is too low to contribute to any static aging effects and the yield drops disappear.

Despite the loss of the static aging effect associated with the high interpass times, the presence of DSA is still quite noticeable on all the flow curves, regardless of temperature and interpass time. This can be explained by the fact that the dislocations

required are generated during the first few percent of renewed straining. It can also be concluded, at least tentatively, that the dislocation density requirement for DSA is much lower than for SSA.

4.1.3 THE EFFECT OF STRAIN RATE

As stated in **Chapter 2**, strain rate governs dislocation velocity. By increasing the strain rate, the dislocation velocity is increased as well. Therefore, it could become increasingly difficult for the solute atoms to keep up with the moving dislocations and effectively pin them. Consequently, any aging effects should begin to disappear as the strain rate is increased. Conversely, decreasing the strain rate should have the opposite effect. Some experiments were conducted by employing higher and lower strain rates with the aim of examining the effects of strain rate on the characteristics of static and dynamic strain aging. The results of these experiments can be seen in **Figures 4.12 to 4.14**. The flow curves were determined at temperatures of 1000 and 1100°C using a pass strain of 0.2. The interpass time was set at 0.01s for all these experiments.

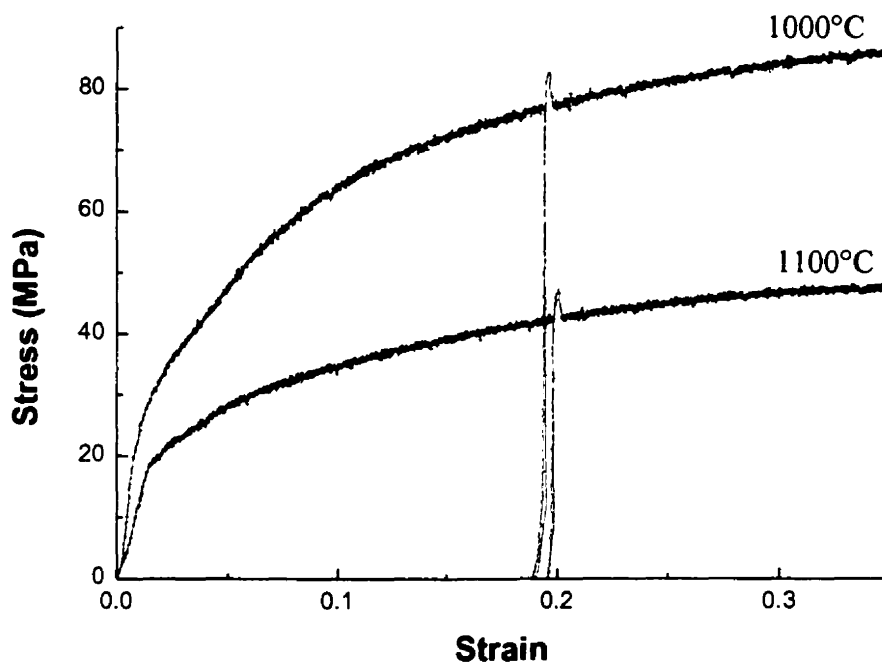


Figure 4.12: Stress-strain curves determined using a strain rate of 0.01 s^{-1} with a pass strain of 0.2 and a 0.01 s interpass time.

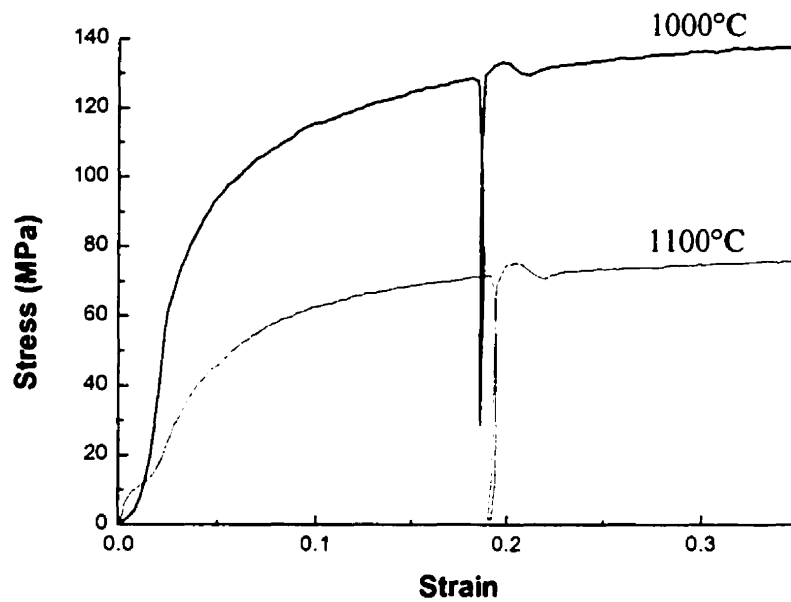


Figure 4.13: Stress-strain curves determined using a strain rate of 1 s^{-1} with a pass strain of 0.2 and a 0.01 s interpass time.

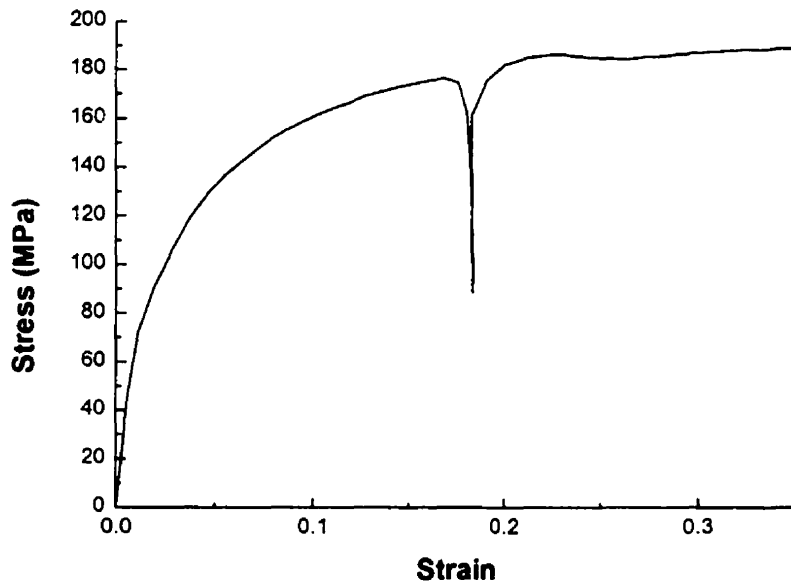


Figure 4.14: Stress-strain curve determined at 1000°C using a strain rate of 5 s^{-1} with a pass strain of 0.2 and a 0.01 s interpass time.

The effects of decreasing the strain rate by more than an order of magnitude, from 0.5 to 0.01 s^{-1} , can be seen in **Figure 4.12**. Again, the effect of temperature on the flow curves is made evident as a decrease in the level of the flow stress. It should also be noted that, by decreasing the strain rate, the flow stress decreases as well. This can be seen when comparing the flow curve at 1000°C and 0.01 s^{-1} with the flow curve at 1000°C and 0.5 s^{-1} (**Figure 4.2**). It can be seen that the SSA yield drops are again present, although they appear to be much sharper than at higher strain rates. The presence of DSA serrations is also highly evident at the lower strain rate. The frequency and intensity of the serrations was increased dramatically by lowering the strain rate to 0.01 s^{-1} . This can be explained in terms of the decrease in the dislocation velocity. As a result, more solute atoms are able to entrap the dislocations, thereby increasing the frequency of dislocation pinning. The strength of the surrounding solute atmosphere also increases, requiring more energy for the dislocations to break free. This can also explain the increase in magnitude of the SSA peaks. The presence of the critical strain, as discussed in **Section 4.1**, is also noticeable on the flow curves of **Figure 4.12**.

The static aging effects are still present when the strain rate is increased from 0.5 to 1 s^{-1} . As opposed to appearing sharper, as they did when the strain rate was reduced, these yield drops appear somewhat broader. It is also clearly evident that the serrations attributable to DSA have disappeared. This can be explained by considering that the dislocation velocity has increased to a point where they have left the solute atoms behind. In this case, the solute atoms are no longer able to accumulate around the dislocations and pin them. However, during the interruption, when dislocation motion is halted, the solute atoms are still able to pin the dislocations to produce the static aging effects. Another effect of increasing the strain rate is that the dislocation density also increases, resulting in an increase in the strength of the material. This can be seen by comparing the flow curves in **Figure 4.13** with those in **Figure 4.2**.

Increasing the strain rate by an order of magnitude, from 0.5 to 5 s^{-1} , has a dramatic effect on the flow curve of steel A (**Figure 4.14**). As was the case when the strain rate was increased to 1 s^{-1} , there are no longer any serrations evident on the flow

curve when increasing the strain rate to 5 s^{-1} . However, the relatively sharp yield drop observed throughout the previous experiments is no longer evident. Nevertheless, by closely examining the flow curve, a slight hump can be noticed, which may be construed as an SSA yield drop. If, in fact, the slight peak is a result of SSA, it can be concluded that any further increase in the strain rate will result in the disappearance of static aging. The disappearance of the serrations is attributed to the increase in dislocation velocity. In this case, the order of magnitude increase in strain rate drastically increases the velocity of the dislocations. Therefore, under this strain rate condition, the dislocations are moving too quickly to be pinned by the slower solute atoms. Since the solute atoms do not hinder dislocation motion, the DSA effects disappear. It can be seen when examining the flow curve generated at a strain rate of 5 s^{-1} (**Figure 4.14**) that there is a noticeable amount of softening that takes place during the interpass time, despite a very fast interpass time of 0.01 s. There is even a slight amount of softening visible on the flow curves obtained at a strain rate of 1 s^{-1} (**Figure 4.13**) and an interpass time of 0.01 s. Comparing these results with those of the flow curves determined at strain rates of 0.5 and 0.01 s^{-1} (**Figures 4.1 to 4.3** and **Figure 4.12**, respectively), it can be seen that there is no indication of any softening at the lower strain rates at similar interpass times. Therefore, it can be concluded that, as the strain rate is increased, the amount of softening increases as well.

4.2 ELEMENTS RESPONSIBLE FOR THE STATIC AND DYNAMIC STRAIN AGING

In this section, the elements that are considered to be responsible for the static and dynamic strain aging effects observed and described in the previous sections will be discussed. Due to the high temperatures involved in the experiments (i.e. $> 800^\circ\text{C}$), it was concluded that substitutional and not interstitial elements are responsible. At temperatures this high, the diffusion rates of interstitial elements such as carbon and nitrogen, those responsible for strain aging effects at lower temperatures, are too high to allow effective interaction with dislocations and to produce aging in this way.

The substitutional elements that might be responsible for the observed effects can be divided into two categories:

- Alloying elements such as chromium, nickel, niobium, silicon, titanium, etc.
- Impurity elements such as phosphorus, sulphur, copper, etc.

Firstly, the diffusion rates of these elements were examined. The diffusivities of substitutional elements in γ -Fe at elevated temperatures were compared with those of interstitial elements in α -Fe in **Figure 2.10**. It can be seen that the diffusivities of C and N in the low temperature interstitial DSA range fall between 10^{-16} and 2×10^{-14} m²/s. The diffusivities of the substitutional elements are therefore expected to fall in this range at the higher temperatures if they are to produce equivalent strain aging effects. From **Figure 2.10**, it can be seen that the elements Ni, Cr, Mn and P satisfy this condition. However, the elements Si and S lie outside the necessary diffusivity range and can be excluded, at least on the basis of this criterion.

Information regarding the interaction between substitutional elements and steel is also very useful. The interaction or binding energy between solute atoms and dislocations indicates how strongly a given atom is attracted to dislocations and also the severity with which it locks it. For example, a high binding energy implies that the atom has a strong affinity for dislocations and, consequently, it will have a higher pinning effect than an element with a lower binding energy. This means that a dislocation will have more difficulty breaking away from atoms with high interaction energies than those with low interaction energies. Although the interaction energies between solute atoms and *dislocations* are not fully known, the binding energies of solute atoms and grain boundaries in γ -Fe are available for certain elements. It is assumed here that these values are comparable to the binding energy between solute atoms and dislocations. The binding energy values of selected elements are listed in **Table 4.2**.

Table 4.2: Binding energies between solute atoms and grain boundaries in γ -Fe⁴⁷.

Element	Binding Energy (kJ/mole)
Mo	-20
Nb	-20
P	-55
S	-88
Si	-17

Sulphur followed by phosphorus have the highest binding energies. They possess values of -88 and -55 kJ/mole, respectively. These levels are much higher than any of the other values presented in **Table 4.2**. When these values are combined with the diffusivities obtained from **Figure 2.10**, it is evident that S, Si and P all have the attributes necessary to produce strain aging effects. However, as was previously mentioned, the diffusivities of S and Si exceed the target diffusivity range and have therefore been omitted here. This leaves the element phosphorus as the primary candidate responsible for the observed effect.

Based on the chemical composition of steel A, listed in **Table 3.1**, it is reasonable to assume that the elements Cr and Ni could also contribute to the strain aging effects observed due to their high concentrations within the material. They comprise 18.41 and 8.21 % of steel A by weight, respectively. Their diffusivities also fall within the range discussed above. When these two factors are combined, Cr and Ni become additional possible candidates.

By analysing the concentrations, binding energies and diffusivities of the elements contained within steel A, three elements were isolated for further consideration. These are the elements chromium, nickel and phosphorus, which are considered as perhaps responsible for the static and dynamic strain aging effects observed while testing. To throw further light on which of these elements might be responsible, certain diffusion calculations were performed. These are outlined in the following section.

4.2.1 DIFFUSION CALCULATIONS

To determine if the aforementioned elements are responsible for the static strain aging yield drops, it is necessary to know:

- The distance between dislocations.
- The distance a solute atom can travel by diffusion during the interpass time.

These values will indicate whether it is theoretically possible for these elements to travel the necessary distance and pin the dislocations during the relatively short interpass times encountered during experimentation. The necessary values can be calculated using the dislocation density, ρ . The average inter-dislocation distance, \bar{l} , can be determined as follows:

$$\bar{l} \approx \frac{1}{\sqrt{\rho}} \quad (4.2)$$

It can be seen that the distance between dislocations is dependent upon the dislocation density. The dislocation density can be calculated using the following formula⁴³:

$$\Delta\sigma = \alpha\mu b\sqrt{\rho} \quad (4.3)$$

or

$$\Delta\sigma = k\sqrt{\rho} \quad (4.4)$$

where $\Delta\sigma$ is the amount of work hardening. It is the difference between the maximum stress before unloading and the initial yield stress on a flow curve (i.e. $\sigma_m - \sigma_o$ in **Equation 4.1**). The term k is a constant of proportionality equal to $\alpha\mu b$, where α is a constant, μ is the shear modulus and b is the Burgers vector. The constant of proportionality has a value of about 20 N/m.

Using the previous equations and values, the average inter-dislocation distance was calculated for pass strains of 0.1 and 0.2. The average distance between dislocations was found to be approximately:

- 300 nm at a pass strain of 0.2.
- 500 nm at a pass strain of 0.1.

It can be seen that the inter-dislocation distance decreases when the pass strain is increased to 0.2. This is due to the fact that the dislocation density has increased, so that there are more dislocations within the same volume.

It is important to note that the distance calculated above is the distance from one dislocation to another. In reality, a solute atom will only have to travel a maximum of half the calculated distance or:

- 150 nm at a pass strain of 0.2.
- 250 nm at a pass strain of 0.1.

Now that the distance between dislocations has been established, it is necessary to determine whether the solute atoms are able to travel these distances within the time available. The mean distance an atom can travel by diffusion, \bar{X} , during a given time, t , is determined as follows:

$$\bar{X} = \sqrt{2Dt} \quad (4.5)$$

where D is the diffusivity of the selected atom. The mean distances were calculated for the elements Cr, Ni and P at temperatures of 1000 and 1100°C for the various interpass times used in the experiments. These results are presented graphically in **Figures 4.15** and **4.16** below.

The effect of temperature on diffusion rate is clearly visible from the figures below. As the temperature is increased, the atoms are able to travel much greater distances. It is also evident that phosphorus is able to travel much greater distances than chromium or nickel during the same amount of time. This was also evident in **Figure 2.10**, as P had a greater diffusivity than either Cr or Ni. The dashed lines on **Figures 4.15** and **4.16** represent the maximum distances the atoms need to travel to interact with the dislocations at pass strains of 0.2 and 0.1, i.e. 150 and 250 nm, respectively. In the case of Cr and Ni, it is possible for these atoms to reach the dislocations, but only at relatively high interpass times and temperatures. In fact, at 1000°C, Ni atoms are not able to diffuse to the dislocations during any of the experimental interpass times. The Cr atoms are able to diffuse the distance that corresponds to a pass strain of 0.2, but only at

interpass times approaching 50 s. The P atoms attain these distances much more easily. However, the interpass times required are still higher than 0.01s, the interval after which the first SSA yield drops were visible. Nevertheless, at 1200°C, the Cr atoms are able to diffuse almost as quickly as the P atoms do at 1100°C.

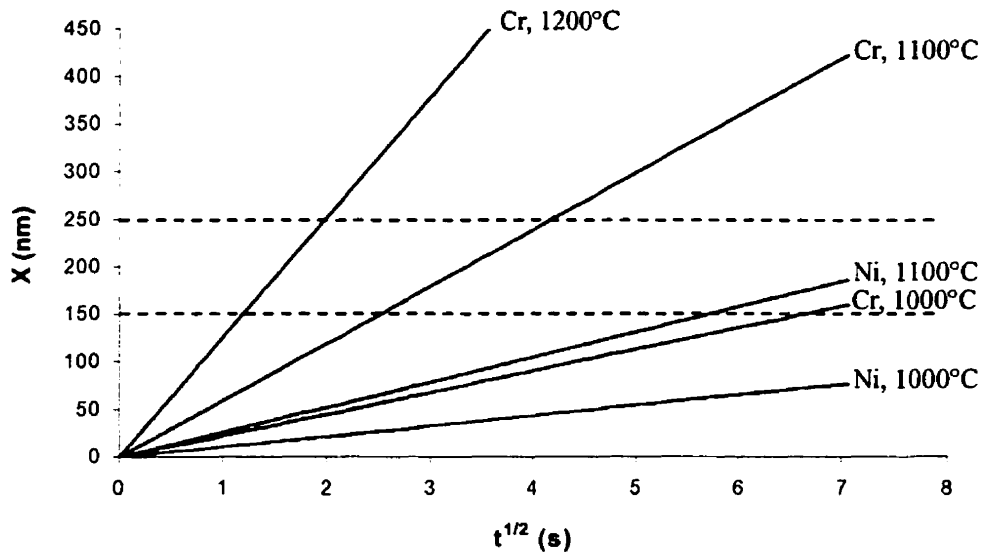


Figure 4.15: Mean distances travelled by Cr and Ni atoms during the experimental interpass times.

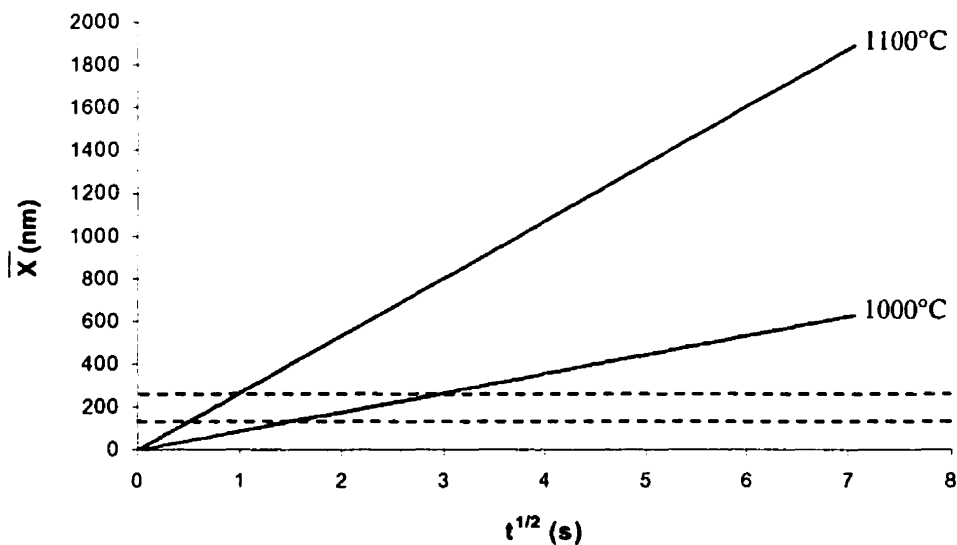


Figure 4.16: Mean distances travelled by P atoms during the experimental interpass times.

Therefore, it has been established that these atoms are able to travel the required distances, but only during relatively long interpass times. However, as previously stated, static aging effects were visible after interpass times as short as 0.01 s. One possible explanation is that the atoms may have been close to a dislocation and did not have to travel very far. It was said that the *maximum* distance the atoms have to travel was half the inter-dislocation distance. If the atoms were closer than half the inter-dislocation distance, then the diffusion time would be decreased in accordance with their proximity to the dislocations. In certain cases, it would then be possible to reach the dislocations during extremely short periods of time. Another possible explanation involves enhanced diffusion of the substitutional solute atoms as a result of the presence of deformation-induced vacancies. Basically, when a metal is deformed, vacancies are produced. Since the mode of diffusion for substitutional atoms is vacancy diffusion, increasing the concentration of available vacancies will increase the diffusion rate. This theory will be further explored in a subsequent section.

4.3 SIMPLE COMPRESSION RESULTS FOR STEEL B

A second series of compression tests was performed using steel B. The first series of tests was conducted using steel A and was discussed in **Section 4.1**. Steel B was an extremely pure stainless steel. As seen from its chemical composition, listed in **Table 3.1**, only the major alloying elements were present to any significant degree. These elements, Cr and Ni, comprised 18 and 12 wt.% of the steel, respectively. All the other elements combined, both alloying and impurity (i.e. C, N, P, S, etc.), had a total concentration of less than 15 ppm. As stated in the previous section, Cr and Ni are the two substitutional alloying elements that could conceivably be responsible for the aging effects observed when testing steel A. Therefore steel B, in which only these elements were present, was used to determine if these were indeed responsible for the observed aging phenomena. Unfortunately, due to the high cost and difficulty of producing this type of steel, only a limited number of samples were obtained. Thus, the test parameters were carefully chosen based on the results from steel A. Basically, these were the ones associated with strong evidence of strain aging. The test temperatures fell between 900

and 1200°C. A strain rate of 0.5 s^{-1} with a 0.2 applied pass strain were also used. The flow curves determined on steel B can be seen in Figures 4.17 to 4.20.

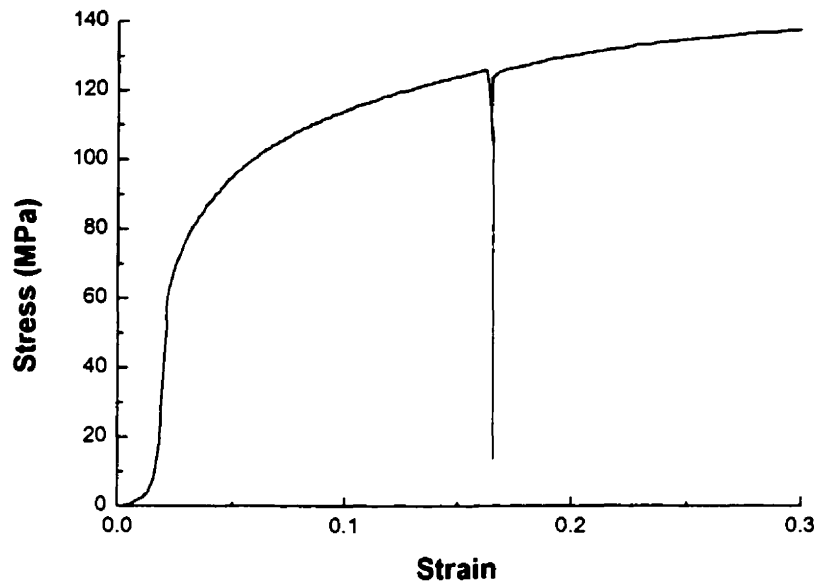


Figure 4.17: Stress-strain curve of steel B determined at 900°C; strain rate = 0.5 s^{-1} ; pass strain = 0.2; interpass time = 0.01 s.

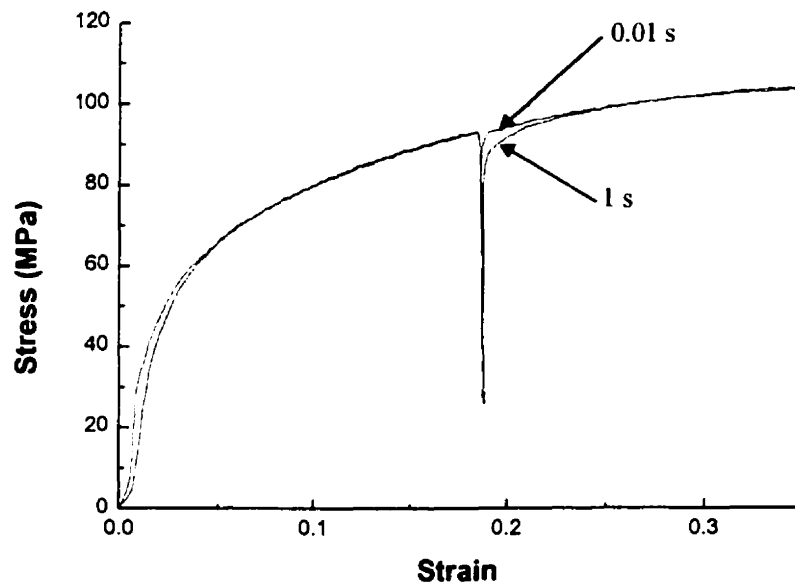


Figure 4.18: Stress-strain curves of steel B determined at 1000°C; strain rate = 0.5 s^{-1} ; pass strain = 0.2; interpass times = 0.01 and 1 s.

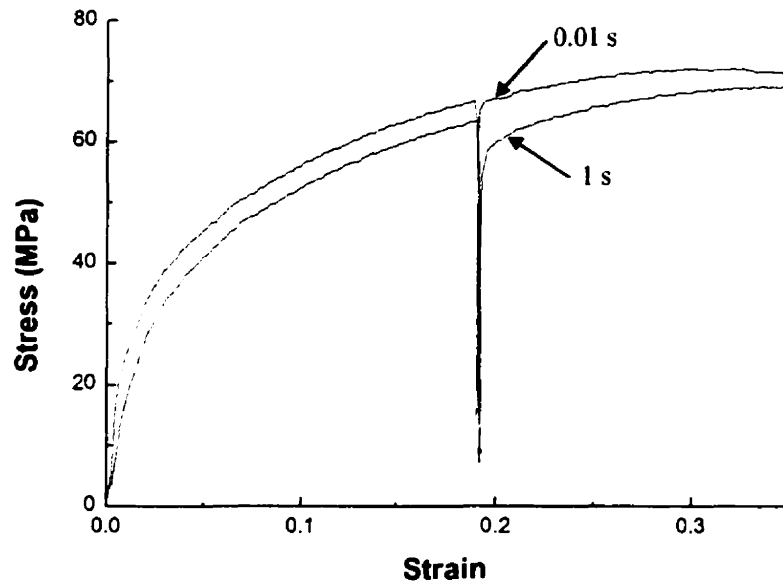


Figure 4.19: Stress-strain curves of steel B determined at 1100°C; strain rate = 0.5 s^{-1} ; pass strain = 0.2; interpass times = 0.01 and 1 s.

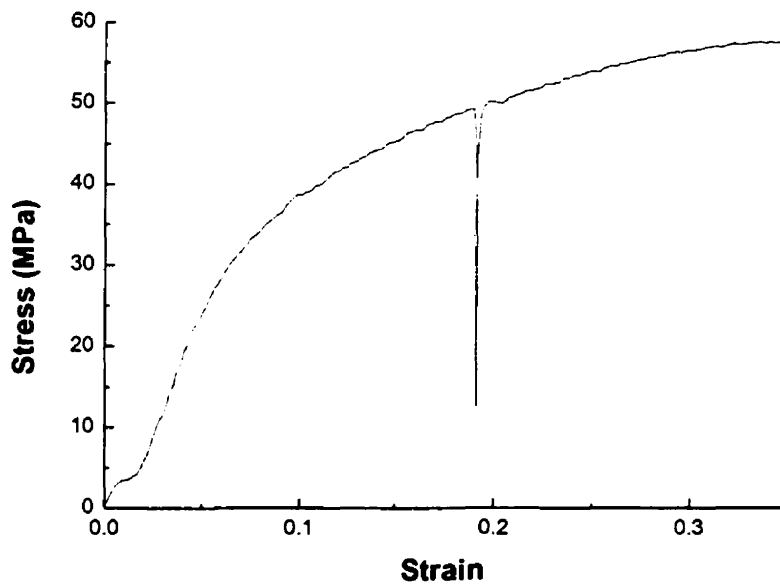


Figure 4.20: Stress-strain curve for steel B determined at 1200°C; strain rate = 0.5 s^{-1} ; pass strain = 0.2; interpass time = 0.01 s.

The most important thing to be noted when examining **Figures 4.17 to 4.20** is that the yield drops attributable to static strain aging are no longer clearly visible. There does appear to be a small yield drop at 1200°C (**Figure 4.20**) and the reloading flow stress level remains high, despite the high temperature. This can perhaps be justified by observing that the Cr diffusion rate at 1200°C is approximately equal to that of P at 1100°C, see **Figure 4.15**. From these observations, it can be concluded that the major alloying elements, Cr and Ni, are not responsible for the SSA observed at 1000 and 1100°C. The most reasonable explanation for this conclusion relates to their diffusivities. As pointed out in the previous section on diffusion, Cr and Ni are not able to diffuse the required distances at 1000 and 1100°C to interact with the dislocations during the given interpass times. Therefore, no static aging is possible at those temperatures. This general statement may not, however, apply at 1200°C.

Even when the interpass time was increased from 0.01 to 1s, allowing more time for solute diffusion, no SSA was observed. As was the case with the experimental results from steel A, increasing interpass time results in increased softening. However, the amount of softening is not as high as expected, especially at the higher temperatures. This is related to the absence of deformation vacancies, as discussed in **Section 4.1.2**.

With regard to DSA, there are slight serrations visible on all the steel B flow curves. However, these serrations are not as prominent as they were in the previous experiments carried out on steel A. In addition, given that Cr and Ni could not induce SSA, it seems unlikely that these elements will then contribute to DSA. Therefore, it was assumed that the serrations present on these flow curves were caused by machine noise. While the latter remains a possible cause for the appearance of serrations, the likelihood that smaller amounts of DSA are caused by Cr and Ni should not be fully discounted. Since dislocations and solute atoms are both moving through the lattice during deformation, moments could arise when dislocations and solute atoms come close enough to each other to interact. This may be happening, for example, at 1200°C.

The results obtained from the experiments carried out using steel B suggest that Cr and Ni are not responsible for the SSA and DSA phenomena observed when testing steel A (i.e. at 1000 and 1100C). However, a slight probability exists that Cr may contribute to limited DSA, particularly at the highest temperature. By eliminating Cr and Ni as being responsible for the steel A phenomena, other elements such Cu, Mn and Mo can also be discounted because they possess similar diffusion coefficients and can be expected to behave in similar ways. This leaves P as the most likely candidate responsible for the SSA and DSA observed here. This conclusion is supported by the fact that P possesses both a high binding energy combined with a high diffusivity.

4.4 ENHANCED DIFFUSION

As suggested in previous sections, enhanced diffusion might play a role in explaining the presence of static aging after very short interpass times. When a material is deformed, excess vacancies are produced at dislocation jogs. At high temperatures, there is an increased effect due to the increased concentration of thermal jogs. Since the diffusion mode for substitutional elements is by vacancy diffusion, increasing the vacancy concentration will increase the diffusion rate as well (the latter increases with the vacancy concentration). It was shown in the work of Militzer *et al.* that, at high strain rates ($> 0.1 \text{ s}^{-1}$), as the strain rate is increased, diffusion is enhanced as a result of the progressively higher excess vacancy concentration⁴⁸. In fact, it was suggested that the excess vacancy concentrations might attain levels 2 to 3 orders of magnitude higher than at equilibrium. These excess vacancies, generated as the metal is deformed, result in the more rapid diffusion of solute atoms through the lattice. Therefore, this could explain the appearance of DSA serrations all along the flow curves of steel A. However, once deformation has ceased, these excess vacancies possess extremely short lifetimes, as can be seen in **Figure 4.21**.

Here, the y-axis is a measure of the concentration of excess vacancies, where C_{ex} is the excess vacancy concentration and C_{th} is the steady state or equilibrium vacancy concentration. From **Figure 4.21**, it can be seen that the maximum strain rate employed in the calculations was 0.1 s^{-1} . The strain rate employed for the majority of the

experiments on steel A was 0.5 s^{-1} , which is slightly higher. Regardless, it can be seen that, at that strain rate, the excess vacancy concentration is expected to increase by approximately an order of magnitude. Once deformation is stopped, the excess vacancies survive for less than one second. In the present work, SSA was observed after interpass times of 0.01, 0.1 and 1 s. Therefore, the presence of excess vacancies appears to enhance the diffusion rates of the solute elements so that they are able to travel to the dislocations during these very short interpass times. The deformation vacancies can also explain the effects observed when the interpass time was increased. As the latter is increased, the concentration of excess vacancies decreases concurrently. Consequently, the diffusion rate of the solutes decreases as well. Eventually, the solutes are no longer able to migrate to the dislocations and the aging effects disappear.

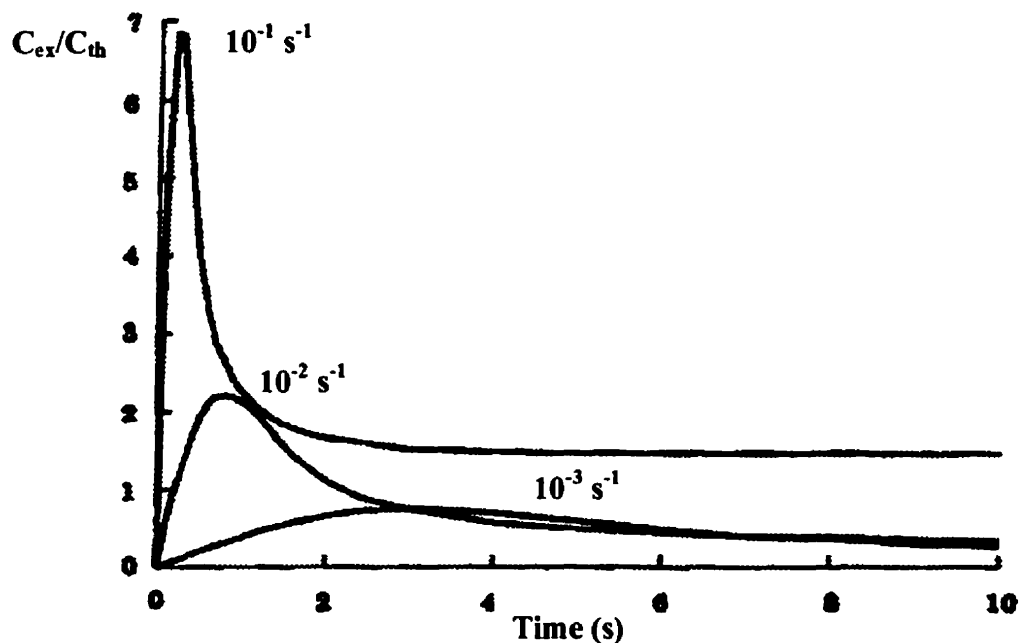


Figure 4.21: Time dependence of the excess vacancy concentration⁴⁸.

4.5 COMPLEX FORMATION AND NON-EQUILIBRIUM SEGREGATION

Another explanation for the strain aging effects observed involves the formation of complexes, resulting in the non-equilibrium temporary segregation of solute atoms on

dislocations. As stated in the previous section, deformation produces vacancies at dislocation jogs. It has been shown that certain atoms, such as boron, combine with these vacancies to produce complexes, such as boron-vacancy (B-V) complexes^{46, 48-53}. It is possible that phosphorus behaves in the same manner as boron, producing phosphorus-vacancy (P-V) complexes. The diffusivity of the complexes is higher than that of the solute atoms alone⁴⁸. These complexes migrate towards dislocations because the latter act as sinks for the complexes. During continuous deformation, the complexes are annihilated, the rate of which depends on the rate of absorption of the vacancies by the dislocations. This dynamic absorption of the vacancies leads to a supersaturation of the solute atoms on the dislocations. The increased concentration of solute atoms around the dislocations leads to DSA during deformation at high temperatures. When deformation ceases, vacancies begin to disappear, as was discussed in the previous section. This results in a rapid and temporary segregation of the solute atoms around the stationary dislocations. Such an increased concentration of impurity atoms could lead to the SSA effects observed when straining is resumed. However, since the increased concentration is of the non-equilibrium variety, it decreases with time until the equilibrium value is attained. At this point, the concentration of solute elements is insufficient to produce SSA.

4.6 STRAIN RATE CHANGE RESULTS

In an attempt to obtain further proof for the occurrence of DSA, strain rate change tests were conducted. Basically, this test was designed to determine whether a material exhibits positive or negative strain rate sensitivity under the experimental conditions employed. As was discussed in **Chapter 2**, negative strain rate sensitivity (SRS) is a good indication of the presence of DSA. As can be seen from **Figure 2.8**, when in the negative SRS region, increasing the strain rate should result in a *decrease* in the flow stress. Conversely, if the strain rate is decreased into this region, an *increase* in the flow stress should be observed.

Strain rate change tests were conducted at a temperature of 1000°C. These tests were carried out by increasing and decreasing the strain rate. The results of these experiments can be seen in **Figures 4.22 to 4.24**.

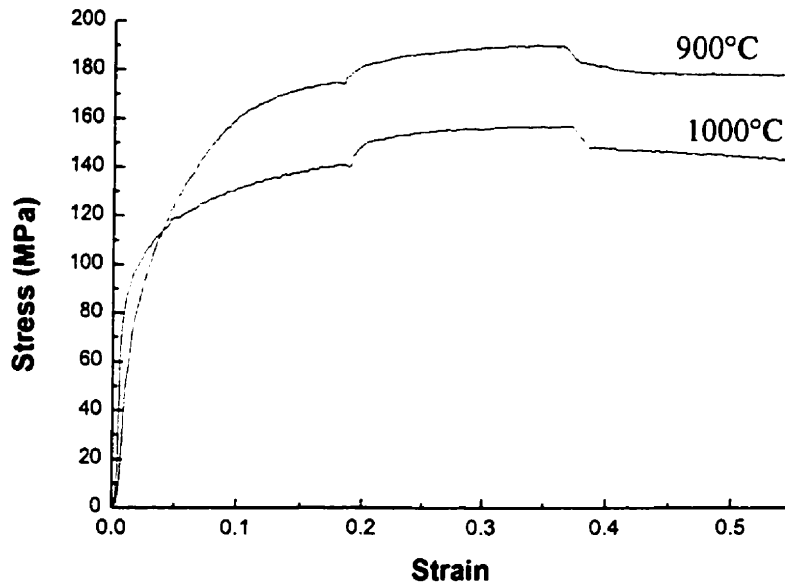


Figure 4.22: Stress-strain curves determined in the strain rate change tests: 0.5 to 1 and then back to 0.5 s⁻¹.

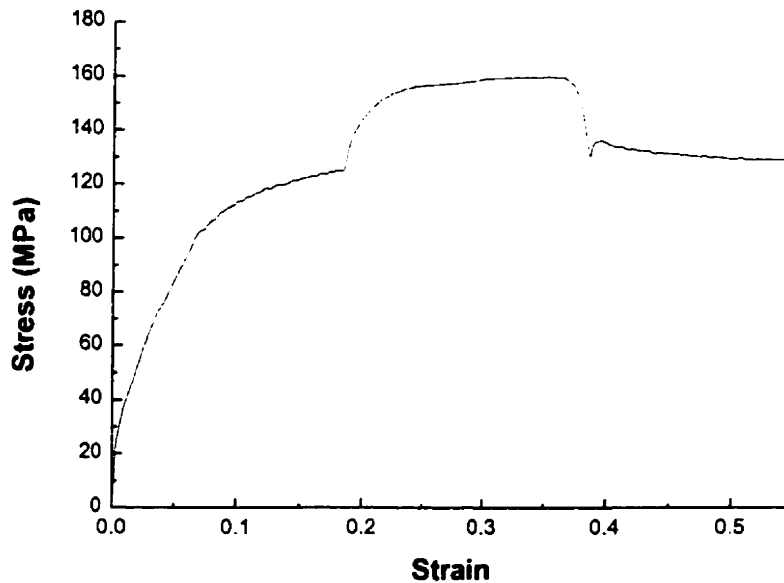


Figure 4.23: Stress-strain curve determined in the strain rate change test at 1000°C: 0.5 to 5 and then back to 0.5 s⁻¹.

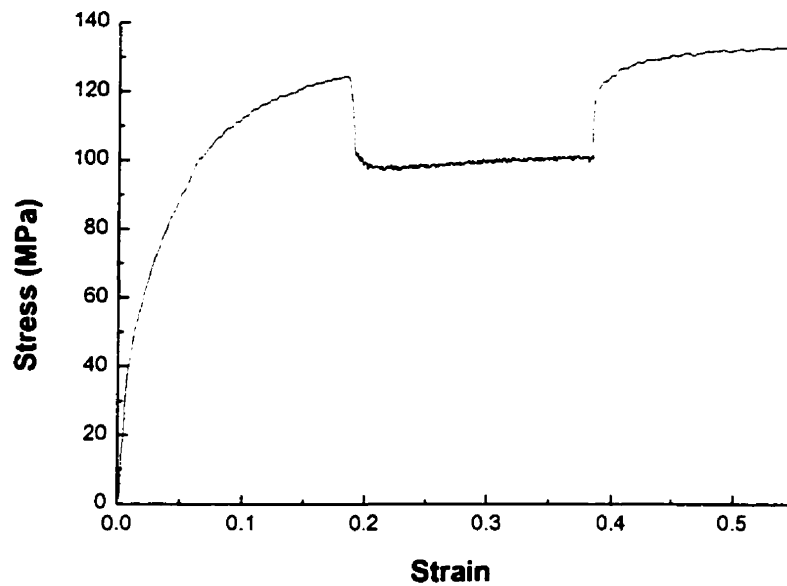


Figure 4.24: Stress-strain curve determined in the strain rate change test at 1000°C: 0.5 to 0.05 and then back to 0.5 s⁻¹.

Figures 4.22 and 4.23 display the results obtained when the strain rate was increased, while Figure 4.24 shows a test result for a strain rate decrease. When increasing the strain rate from 0.5 to 1 s⁻¹ and 0.5 to 5 s⁻¹, an increase in flow stress was observed. Similarly, when decreasing the strain rate from 0.5 to 0.05 s⁻¹, a decrease in the flow stress was observed. These results indicate that the SRS is positive as opposed to a negative SRS, as was originally expected.

A possible explanation for the appearance of a positive SRS rather than a negative SRS may be postulated by extrapolating Figure 2.8 to higher temperatures. At higher temperatures, the differences between the high and low strain rate curves for the pure material increase significantly. The characteristic “hump” associated with the materials that exhibit DSA is smaller than at lower temperatures. Therefore, it is possible that these curves do not intersect as they do at lower temperatures. This indicates that no negative SRS is possible at the higher temperatures, as was observed in these experiments.

However, to prove such results would require extensive experimentation, which was beyond the scope of this study.

CHAPTER 5

CONCLUSIONS

The purpose of this study was to examine the high temperature strain aging behavior of a typical 304 stainless steel. It was hypothesized that, at elevated temperatures, substitutional elements are responsible for both static and dynamic strain aging. Various experiments were designed in an attempt to extract evidence regarding these phenomena. The following conclusions were derived from this study.

1. Yield drops attributable to static strain aging (SSA) and serrated yielding associated with dynamic strain aging (DSA) were visible on all the high temperature flow curves determined on a 304 type stainless steel (steel A). These aging effects appear over the temperature range from 850°C to 1200°C.
2. The yield drops and serrations disappeared when the testing temperature was lowered to 800°C. Therefore the lower temperature limit for the appearance of yield drops and serrations occurs between 800 and 850°C.
 - Increased temperatures result in an increase in the size of the SSA yield drops.

- The appearance of serrations is preceded by a particular strain, known as the “critical strain”. Prior to this strain, the flow curve is fairly smooth and no prominent serrations are visible.
3. The occurrence of SSA is dependent upon the pass strain applied. By applying a pass strain of 0.2, SSA is readily visible.
 - Lowering the pass strain to 0.1 results in the disappearance of SSA. This can be explained by the change in the dislocation density. By lowering the applied strain, the dislocation density is also lowered. Therefore, insufficient dislocations (and perhaps deformation vacancies) are present to produce SSA.
 - By applying a 0.4 pass strain, SSA disappears. However, in this instance, the loss of SSA is probably attributable to an excess of deformation vacancies.
 - It should be noted that two passes at a strain of 0.1 are not equivalent to a single pass using a strain of 0.2. This may involve the loss of some deformation vacancies during the interpass time.
 4. Increasing the interpass time results in a decrease in the amplitude of the SSA yield drop. If the interpass time is long enough, SSA disappears altogether. This loss of SSA is readily associated with a decrease in the concentration of deformation vacancies.
 5. Varying the strain rate affects the appearance of SSA and DSA.
 - Decreasing the strain rate increases the intensity of the SSA yield drops and increases the intensity and frequency of the DSA serrations. This seems to result from the decrease in the dislocation velocity.
 - Increasing the strain rate results in a progressive decline in the presence of both SSA and DSA. In fact, the serrations disappeared at a strain rate of 1 s^{-1} , while yield drops were virtually non-existent at a strain rate of 5 s^{-1} . This may be explained by a significant increase in the dislocation velocity.

6. Substitutional elements appear to be responsible for these two types of effects. At these high temperatures, the diffusivities of certain substitutional atoms rival those of carbon and nitrogen within the blue brittle region (100 to 300°C). The elements that may be responsible are:
 - Cr and Ni due to their diffusivities and relatively high concentrations within the specimens.
 - P due to its high diffusivity and high binding energy.

7. Pure 304 stainless steel containing only Cr and Ni was tested under the same conditions that led to the ready observation of SSA and DSA.
 - Under these conditions, no yield drops were visible at 1000 and 1100°C.
 - Some possible serrations were visible on the flow curves, but this may have been caused by machine noise.
 - Cr and Ni can be eliminated as possible candidates of the SSA and DSA phenomena observed at 1000 and 1100°C. Nevertheless, Cr appears to be a possible candidate at 1200°C.
 - Due to its high diffusivity combined with its high binding energy, P appears to be the most likely candidate responsible for the SSA and DSA effects observed at elevated temperatures.

8. There are two possible explanations regarding the presence of SSA after holding for very short times.
 - The first is enhanced diffusion as a result of the presence of deformation-induced vacancies. The excess vacancies generated during straining can enhance the diffusion rate of solute elements by an order of magnitude. Despite their extremely short lifetimes, once deformation is halted, these excess vacancies exist long enough to contribute to SSA (and more generalized dislocation pinning) during interpass times below 1 s.
 - The second theory, which is linked to the first, is that of complex formation leading to non-equilibrium segregation. According to this view, impurity elements, such as P, combine with the vacancies (V) generated during deformation

to produce P-V complexes. These complexes migrate towards dislocation "sinks" and are eventually absorbed. This leads to an increased non-equilibrium concentration of the impurity atoms on the stationary dislocations. This sequence of events results in SSA upon renewed straining. According to this view, the disappearance of the yield drops simply arises from the "evaporation" or disappearance of the non-equilibrium segregation once the vacancies are liberated from the complexes.

Although this study provided some evidence for the occurrence of static and dynamic strain aging caused by substitutional elements at high temperatures, more information is required to fully characterize these phenomena. The ultimate goal of this study was to determine the ranges (i.e. the temperature and strain rate ranges) within which DSA and SSA occur. However, due to time constraints, testing was limited. More work must therefore be conducted to fully investigate the presence of SSA and DSA at high temperatures. Such research seems to have a promising future.

REFERENCES

1. J.D. Baird, "Chapter 8: Dynamic Strain Aging" in The Inhomogeneity of Plastic Deformation, ASM, 1973, p. 191.
2. J.M. Robinson and M.P. Shaw, *International Materials Reviews*, V. 39, No. 3, 1994, p. 113.
3. A. Portevin and F. LeChatelier, *Comp. Rend. Acad. Sc.*, V. 176, 1923, p. 507.
4. S. Lou and D.O. Northwood, *Materials Forum*, V. 17, No. 2, 1993, p. 153.
5. A. Kirihata, F. Siciliano Jr., T.M. Maccagno and J.J. Jonas, *Iron and Steel Institute of Japan International*, V. 38, No. 2, 1998, p. 187.
6. D.Q. Bai, J.J. Jonas, P.R. Hastings and N. Nickeloletopoulos, *Metallurgical Transactions*, V. 29A, No. 5, 1998, p. 1384.
7. G.E. Dieter, Mechanical Metallurgy, Third Edition, McGraw-Hill, 1986.
8. A.H. Cottrell, Dislocations and Plastic Flow in Crystals, Oxford University Press, 1953.
9. J.D. Baird, *Iron and Steel*, May 1963, p. 186.
10. A.S. Keh, Y. Nakada and W.C. Leslie, "Dynamic Strain Aging in Iron and Steel" in Dislocation Dynamics, McGraw-Hill, 1968, p. 381.
11. J.D. Baird, *Iron and Steel*, July 1963, p. 326.
12. B.B. Hundy, *Metallurgia*, V. 53, 1956, p. 203.
13. D.V. Wilson and B. Russell, *Acta Metallurgica*, V. 8, 1960, p. 36.
14. D.V. Wilson and B. Russell, *Acta Metallurgica*, V. 8, 1960, p. 468.
15. C.C. Li and W.C. Leslie, *Metallurgical Transactions*, V.9A, No. 12, 1978, p. 1765.
16. D. Blanc and J.L. Strudel, Proceedings of the 7th International Conference on the Strength of Metals and Alloys, Pergamon Press, p. 349.
17. G.H. Rubiolo and P.B. Bozzano, *Materials Transactions, JIM*, V. 36, No. 9, 1995, p. 1124.

References

18. P. Hähner, *Materials Science and Engineering A*, V. 207, No. 2, 1996, p. 208.
19. K.J. Draheim and J. Schlipf, *Computational Materials Science*, V. 5, No. 1, 1996, p. 67.
20. J.D. Baird, *Metallurgical Reviews*, Review 149, V. 16, 1971, p. 1.
21. N.E. Zeghib and J.R. Klepaczko, *Journal of Material Science*, V. 31, No. 22, 1996, p. 6085.
22. A. Karimi Taheri, T.M. Maccagno and J.J. Jonas, *Iron and Steel Institute of Japan International*, V. 35, No. 12, 1995, p. 1532.
23. O.N. Senkov and J.J. Jonas, *Metallurgical and Materials Transactions*, V. 27A, 1996, p. 1877.
24. L.J. Cuddy and W.C. Leslie, *Acta Metallurgica*, V. 20, Oct. 1972, p. 1157.
25. W.R. Thomas and G.M. Leak, *Iron and Steel Institute of Japan*, V. 180, 1955, p. 155.
26. L.H. de Almeida and P.R.O. Emygdio, *Scripta Metallurgica et Materialia*, V. 31, No. 5, 1994, p. 505.
27. P. Rodriguez, *Bulletin of Materials Science*, V. 6, No. 4, 1984, p. 653.
28. M.R. Winstone and R.D. Rawlings, *Journal of Materials Science*, V. 6, 1971, p. 1355.
29. A.H. Cottrell, *Philosophical Magazine*, V. 44, 1953, p. 829.
30. P.J. Worthington and B.J. Brindley, *Philosophical Magazine*, V. 19, 1969, p. 1175.
31. S.L. Mannan, K.G. Samuel and P. Rodriguez, International Conference on the Strength of Metals and Alloys (ICSMA 6), V. 2, Pergamon Press, 1982, p. 637.
32. M.L. Weaver, *Materials Research Society Symposium Proceedings*, V. 460, 1997, p. 499.
33. L.P. Kubin and Y. Estrin, *Scripta Metallurgica*, V. 23, 1989, p. 815.
34. L.P. Kubin and Y. Estrin, *Acta Metallurgica and Materialia*, V. 38, 1990, p. 697.
35. S. Cunningham, M. Eng. Thesis, McGill University, 1999
36. J.D. Baird, and A. Jamieson, *Iron and Steel Institute of Japan*, V. 204, 1966, p.793.

References

37. C. Weidig, M. Espindola, B. Gonzalez, P. Rodrigues and M. Andrade, *Wire Journal International*, V. 28, No. 1, 1985 p. 82.
38. A. Karimi Taheri, T.M. Maccagno and J.J. Jonas, *Metallurgical and Materials Transactions A*, V. 26A, 1995, p. 1183.
39. W.F. Hosford and R.M. Caddell, Metal Forming: Mechanics and Metallurgy, Second Edition, PTR Prentice Hall inc., 1993.
40. www.inaba.nrm.go.jp/diff.
41. P.S. Follansbee, "High Strain Rate Compression Testing" in Metals Handbook 9th Edition, V. 8, ASM, 1985, p.190.
42. A. Di Chiro, M. Eng. Thesis, McGill University, 1997.
43. R.E. Reed-Hill and R. Abbaschian, Physical Metallurgy Principles, Third Edition, PWS-Kent Publishing Company, 1992.
44. W.D. Callister Jr., Materials Science and Engineering: An Introduction, Third Edition, John Wiley & Sons Inc., 1994.
45. S. Cho, Y. Yoo and J.J. Jonas, *Journal of Materials Science Letters*, in press.
46. X.L. He, M. Djahazi, J.J. Jonas, and J. Jackman, *Acta Metallurgica et Materialia*, V. 39, No. 10, 1991, p. 2295.
47. P. Lejcek and S. Hofmann, *Critical Reviews in Solid State and Materials Science*, V. 20, No. 1, 1995, p. 1.
48. M. Militzer, W.P. Sun and J.J. Jonas, *Acta Metallurgica et Materialia*, V. 42, No. 1, 1994, p. 133.
49. K.T. Aust, R.E. Hanneman, P. Niessen and J.H. Westbrook, *Acta Metallurgica*, V. 16, 1968, p. 291.
50. T.R. Anthony and R.E. Hanneman, *Scripta Metallurgica*, V. 2, 1968, p. 611.
51. T.M. Williams, A.M. Stoneham and D.R. Harries, *Metal Science*, V. 10, 1976, p. 14.
52. M.A.V. Chapman and R.G. Faulkner, *Acta Metallurgica*, V. 31, 1982, p. 677.
53. L. Karlsson, *Acta Metallurgica*, V. 36, 1988, p. 25.